DEUTSCHES ELEKTRONEN-SYNCHROTRON **DESY**

DESY 75/36
September 1975

Study of Photoproduction on Hydrogen in a Streamer Chamber with Tagged Photons for 1.6 GeV < E_γ < 6.3 GeV - Topological and Reaction Cross Sections -

Aachen-Hamburg-Heidelberg-München Collaboration

W. Struczinski
III. Physikalisches Institut der Technischen Hochschule, Aachen

P. Dittmann, V. Eckardt, P. Joos, A. Ladage, H. Meyer, D. Notz
Deutsches Elektronen-Synchrotron DESY, Hamburg

G. Hentschel, J. Knobloch, E. Rabe, H. Taureg
II. Institut für Experimentalphysik der Universität, Hamburg

M. Grimm
Institut für Hochenergiephysik, Heidelberg

I. Derado, P. Schacht, R. Meinke
Max-Planck-Institut für Physik und Astrophysik, München

2 HAMBURG 52 · NOTKESTIEG 1

To be sure that your preprints are promptly included in the
HIGH ENERGY PHYSICS INDEX ,
send them to the following address (if possible by air mail) :

STUDY OF PHOTOPRODUCTION ON HYDROGEN IN A STREAMER CHAMBER WITH TAGGED PHOTONS FOR 1.6 GeV < E_γ < 6.3 GeV

- TOPOLOGICAL AND REACTION CROSS SECTIONS -

Aachen-Hamburg-Heidelberg-München Collaboration

W. Struczinski*

III. Physikalisches Institut der Technischen Hochschule, Aachen.

P. Dittmann**, V. Eckardt**, P. Joos, A. Ladage, H. Meyer, D. Notz**

Deutsches Elektronen Synchrotron DESY, Hamburg.

G. Hentschel**, J. Knobloch, E. Rabe, H. Taureg****

II. Institut für Experimentalphysik der Universität, Hamburg.

M. Grimm

Institut für Hochenergiephysik, Heidelberg.

I. Derado, P. Schacht***, R. Meinke

Max-Planck-Institut für Physik und Astrophysik, München.

* Now at CERN, Geneva, Switzerland.

** Now at Max-Planck-Institut für Physik und Astrophysik, München.

*** Now at SLAC, Stanford, California, USA.

**** Now at Institut für Hochenergiephysik, Heidelberg.

ABSTRACT

We have studied photoproduction using a 1 m streamer chamber at DESY and a tagged photon beam with an energy range of $1.6\ \text{GeV} < E_\gamma < 6.3\ \text{GeV}$. We analysed approximately 30 000 events and report topological, channel and resonance production cross sections for a large number of reactions with three and five outgoing charged particles.

Contents

1. Introduction

2. Experimental procedure
   2.1 Photon beam
   2.2 The streamer chamber
   2.3 The trigger system
   2.4 Scanning and measuring procedure
   2.5 Determination of cross sections

3. Results
   3.1 Topological cross sections
   3.2 Channel cross sections
   3.3 Resonance production in the channel $\gamma p \to p\pi^+\pi^-$
   3.4 " " " " " $\gamma p \to p\pi^+\pi^-\pi^0$
   3.5 " " " " " $\gamma p \to n\pi^+\pi^+\pi^-$
   3.6 " " " " " $\gamma p \to p2\pi^+2\pi^-$
   3.7 " " " " " $\gamma p \to p2\pi^+2\pi^-\pi^0$
   3.8 " " " " " $\gamma p \to n3\pi^+2\pi^-$
   3.9 Resonance production in the channel $\gamma p \to p\pi^+\pi^-$ (+ neutrals)

4. Conclusion
   References
   Tables
   Figure captions
   Figures

1. INTRODUCTION

Photoproduction cross sections for multiparticle processes have been determined in a number of experiments [1,2,3,4,5]. However, in most of the previous experiments there was the difficulty of having a photon beam with a wide energy spectrum and no possibility to measure the photon energy for individual events. Therefore the photon energy could be determined only for the few reactions with no neutrals in the final state (from 3-constraint kinematic fits to the final-state energies and momenta), while for channels with one (or more) neutrals the photon energy was unknown and, since the photon flux depended on energy, no cross sections could be given. Other experiments[3,5] partly overcame this difficulty by using a beam with a narrow energy spectrum, but these measurements were made at only a few discrete energies.

To amend this situation, and to study systematically the energy dependence of the various cross sections, we have undertaken a comprehensive study in which we used an energy-tagged broad band photon beam, together with a 1m long streamer chamber with a built-in hydrogen target, to detect all charged particles in the final state. The laboratory beam energy range covered was 1.6 GeV < E_γ < 6.3 GeV. The photons were produced by bremsstrahlung from monochromatic positrons in a thin radiator, and the momentum of the scattered positrons was measured in a magnetic field with a counter hodoscope to an accuracy of ± 3C MeV. This was amply sufficient for a clean kinematical separation of events with zero, one or more than one neutral particle in the final state.

In section 2 we describe the experiment, and in section 3 the results for topological and channel cross sections are presented as well as for resonance production as obtained from maximum likelihood fits to the mass distributions.

2.EXPERIMENTAL PROCEDURE

2.1.Photon beam

A monochromatic positron beam of energy 6.5,4.3,3.5 or 2.9 GeV and an energy width of 0.5% was hitting a 1.2 mm Al radiator, producing bremsstrahlung. The recoil positrons were momentum analysed with a C Magnet of 21 kGauss and detected in a hodoscope of 12 scintillation counters overlapping each other (photon tagging system, TAG),fig.1. To suppress the background of tridents and knock-on electrons in the radiator we used veto counters on the opposite side of the beam (V3,V6). Processes in which two positrons emerge were vetoed by a veto counter at the end of the tagging system (V4). Photons outside the beam were vetoed by a shower counter with a hole of 3 cm diameter (V5) through which the beam was passing. With this arrangement 92% of all counts in the tagging system were coincident with one high-energy photon. The photon-energy is known, from the recoil momenta, within $\sim\pm1\%$. By triggering the streamer chamber on e^+e^- pairs we could independently measure the energy of the photons for calibration.

We find that in only 8% of the cases the tagging system gave a photon energy more than 90 MeV below the true value.

2.2.The streamer chamber

The double gap streamer chamber [5]) with a sensitive volume of $100\times60\times(2\times16)$ cm^3 was filled with a helium neon mixture (70% Ne,30%He) at atmospheric pressure. By adding a small amount ($\sim10^{-7}$) of electronegative SF_6 the memory time was reduced to 2 μsec. A 400 kV, 10 nsec pulse was applied; it was generated with a 14 stage Marx generator and a 0.8 m coaxial Blumlein system. The streamer chamber was operated in a nearly homogenous magnetic field of 21 kGauss.

Pictures were taken with 3 cameras with a stereo angle of 18^o. The average demagnification was 38; a 35 mm focal length system with f number 2 and Kodak Tri-X Aerographic film SO265 were used.

2.3. The trigger system

The photons passed through a liquid hydrogen target of 3.8 cm length inside the streamer chamber, and were then counted in a totally absorbing shower counter S of 11 rad lengths (fig.2). The target was surrounded by a cylindrical scintillation counter T with a window at the entrance of the beam. This counter counted the particles coming out of the target and simultaneously served as a vacuum container for the target. To veto e^+e^- pair production we used two counters (O,U in fig.2) in a plane through the target and perpendicular to the magnetic field.

The trigger condition for hadronic events was $TAG \cdot T \cdot \bar{S} \cdot \overline{(O + U)}$, for e^+e^- pairs $TAG \cdot T \cdot \bar{S} \cdot O \cdot U$ and the number of "tagged" photons was obtained as the counting rate $TAG \cdot S$.

Data were taken with an intensity of 5-10 thousand tagged photons per sec (= 0.1 MHz).

2.4. Scanning and measuring procedure

The pictures showed so few background tracks that it was possible to scan and measure the pictures in one step. We took 870 000 pictures from which 14 % showed a hadronic event produced by the hydrogen or the targetcounter. Finally we obtained 29 748 events which passed all geometrical and kinematical cuts giving 68 events per μb. Part of the film was scanned twice from which a scanning efficiency of greater than 99 % was found. Since for 9 % of the events one of the charged particles was stopped inside the target scintillator, we measured events with a total charge of the outgoing visible particles $Q = 0$ or 1. The events were measured on conventional bubble chamber film measuring devices and in part on SMP's (Scanning and Measuring Projectors). Geometric reconstruction and kinematic fits were done using the THRESH and GRIND[7]) program chain. Badly measured events were measured twice. Finally 2% of the events remain unmeasurable.

For each particle with momentum below 1 GeV/c for a given mass assignment the ionization predicted from the momentum was checked on the scanning table. The accuracy of themomentum and angle measurements was determined by the average track residual, a measure of the standard deviation of the point coordinate measurement error. It was 7 µm on the film corresponding to 275 µm in real space. Part of thee$^+e^-$ pairs was also measured on a flying spot digitizer[8]. Here we obtained an average track residual of 3.5 µm corresponding to 140 µm.

Before entering the kinematic program GRIND the invisible vertex is reconstructed to separate events originating in the target counter. For this reconstruction at least two visible tracks are needed which precludes an analysis of one prong events. The momenta and angles of the outgoing particles are corrected for energy loss and multiple scattering inside the scintillation counter.

2.5 Determination of cross sections

In this experiment we measure the cross sections for events with at least two outgoing charged particles.The cross sections are determined by counting the events produced in the hydrogen target and dividing by the measured photon flux.

For determining the total cross sections several corrections are necessary:

1. Part of the beam (20 %) did not go through the hydrogen target.
2. Due to double bremsstrahlung 6 % of the events are vetoed by the shower counter.
3. Corrections are also necessary for the deadtime of the shower counter. In the 6.5 GeV run this correction is large (34 %) because the shower counter is counting not only the tagged photons (4.1 GeV < E_γ < 6.3 GeV) but all photons above its threshold (200 MeV).

The results for the total photoproduction cross section corrected for one prong events are within errors in agreement with published data[3,9] over the whole energy range covered (Fig. 3). However, since our systematic uncertainties are of the order of 15 % we prefer to normalize our data to the published total cross sections, or rather to a smooth fit to them.

The expression we use is

$$\sigma_{tot} - \sigma_{1prong} = 98.7\ \mu b + \frac{64.9\ \mu b}{\sqrt{E_\gamma}} - \frac{80\ \mu b}{E_\gamma} \qquad (1),$$

where E_γ is measured in GeV. The first two terms are taken from ref. [10]) and the last one is a fit to the one prong cross section[3]).

3. RESULTS

3.1. Topological cross sections

In order to determine the topological cross sections we use all measured events with a total charge of the outgoing visible tracks Q=0 or 1 and which have their fitted vertex inside the hydrogen target. The unmeasurable events are added for each topology. This number of events must still be corrected for losses due to the veto counters. To do this, each event is rotated around the beam axis by steps of 1^o; if a particle hits one of the veto counters this step is marked. The ratio of marked over unmarked steps gives a weight factor for each event. The resulting corrections are of the order of 20% for two prongs and 15% for five prongs. There is, however, a class of events in which one particle goes nearly in the forward direction ($\theta<2^o$) (θ = angle between outgoing particle and beam); these events are always vetoed and cannot be corrected by the method mentioned above. To correct these losses we plot $\cos\theta$ for all particles. The particles missing near $\cos\theta = 1$ define a correction of 2%.

In our high energy run (E_γ > 4.0 GeV) we used a target counter

of 3 mm scintillator thickness, in the other runs one of 5 mm thickness. The 3 mm counter shows an inefficiency for two minimum ionizing particles of 46% as found from measurements of the e^+e^- pair cross sections. This target counter inefficiency gives large corrections for such three-prong events in which the proton is stopped inside the target (in the very low $|t_{p\to p}|$ region).

The numbers so corrected are added and normalized to the total cross section from formula(1).

In Table 1 we summarize the corrections and uncertainties of the topological cross sections.

In Table 2 and fig.3 the topological cross sections are shown. Within the errors they agree with the results from other experiments.

3.2.Channel cross sections

In this section we discuss the determination of cross sections for four-constraint (4C) events (i.e. events with no outgoing neutral particle), for one-constraint (1C) events (with one neutral particle (π^0,n) or, in the case of an even number of outgoing charged particles, events where the π^+ or p are stopping inside the target counter).
With the kinematic reconstruction program GRIND the following processes are fitted:

$$\left.\begin{array}{l} \gamma p \to p m\pi^+ m\pi^- \\ \gamma p \to p m\pi^+ m\pi^- \pi^0 \\ \gamma p \to n(m+1)\pi^+ m\pi^- \end{array}\right\} \qquad m = 1,2,3$$

i) 4C- events

Events which give a 4 C-fit are accepted if the fit probability was $P(\chi^2) > 0.01$ and if the missing mass squared was zero within the limits.

$$|MM^2| < 3 \cdot \Delta MM^2$$

Each event is checked for the correct ionization. Additional 1 C-fits are disregarded. The number of fitted events is corrected for acceptance losses (see chapter 3.1).

ii) 1C- events with one unmeasured charged particle

If a proton or π^+ stops inside the target counter, the reaction $\gamma p \to p(m\pi^+)(m\pi^-)$ $(m \geq 1)$ gives a one constraint fit. In these cases we check whether the calculated momentum of the missing particle is less than 300 MeV for protons or 200 MeV for pions provided the dip angle of the missing particle is $|\lambda| < 0.72$ rad.

For larger dip angles it is possible for the particle to escape through the target enclosure such that larger momenta are possible.

iii) 1C-events with neutral particles

We now turn to reactions with one kinematic constraint:

$$\gamma p \to p m\pi^+ m\pi^- \pi^0$$
$$\gamma p \to n(m+1)\pi^+ m\pi^-$$

A fit from GRIND is accepted if there is agreement in the observed and calculated ionization, and if the missing mass is correct within two standard deviations-

$$|MM^2 - M^2_{\pi^0(n)}| < 2\,\Delta MM^2 .$$

If there is more than one accepted fit the hypothesis with the smaller missing mass difference divided by the average error $\overline{\Delta MM}$ is accepted:

$$|MM^2 - M^2_{\pi^0}|/\overline{\Delta MM^2_{\pi^0}} \quad \text{or} \quad |MM^2 - M^2_n|/\overline{\Delta MM^2_n} .$$

The estimated uncertainty of this method is 3% for π^0 and 5% for n hypotheses.

The distribution of fit probabilities $P(\chi^2)$ increases below o.2o.This is presumably due to events with two neutrals, giving a spurious (albeit bad) 1C fit. We correct the number of events accordingly by taking the number of events for $P(\chi^2) > 0.20$ and multiplying this number by 1.25. The difference of the uncorrected and corrected event numbers is added to the number of unfitted (multineutral) events.

The numbers are then corrected for acceptance losses ($\sim$ 2%).

At low squared four momentum transfer t from the photon to the $\pi^+\pi^-\pi^0$ system we lose events in which the proton stops inside the target counter. These losses are corrected with the help of the t-distribution $d\sigma/dt$ for events with $m_{\pi^+\pi^-\pi^0} < 1.0$ GeV; the missing events at low t are corrected and the corresponding number of events is subtracted from the unfitted events with one unobserved track.

iv) Unfitted events

Reactions with more than one neutral particle, like

$$\gamma p \to p m\pi^+ m\pi^- k\pi^0, \; k \geq 2$$
$$\gamma p \to n(m+1)\pi^+ m\pi^- \ell\pi^0, \; \ell \geq 1$$

cannot be fitted. For these events we require the missing mass to be larger than the mass of the supposedly missing particles (within errors):

$$|MM^2 + 2\Delta MM^2| > (2\, M_{\pi^0})^2$$
$$|MM^2 + 2\Delta MM^2| > (M_n + M_{\pi^0})^2$$

Ambiguities between several possible hypotheses cannot be resolved in this case.

The cross sections are given in Table 3.

Our results are shown in figs. 4-7 together with the cross sections from other experiments.

3.3 Resonance production in the channel $\gamma p \to p\pi^+\pi^-$

In the following sections we describe the procedure to obtain the resonance production cross sections for reactions having three or five charged particles in the final state.

It should be noted that the cross sections depend on the hypothesis taken into account. Therefore systematical errors could be much higher than statistical errors. In our results only statistical errors are given.

The channel $\gamma p \to p\pi^+\pi^-$ is dominated by ρ^0 production and at lower energies by $\Delta^{++}(1236)$ production. Above $E_\gamma = 2.3$ GeV we observe some f^0 production. In figs. 8 and 9 we show the distribution of

the effective masses for $M_{\pi^+\pi^-}$ and $M_{p\pi^+}$.

The Dalitz plot shows that the events in the ρ^0 region are not equally distributed in the $p\pi^+$-mass. This means that the π^+ is not isotropic in the ρ^0 helicity system but has a decay angular distribution $W(\cos\theta_H,\phi_H) \sim \sin^2\theta_H$. ($\cos\theta_H,\phi_H$ are the polar and azimuth angle in the helicity system).

The distribution of the momentum transfer $d\sigma/d|t|(\gamma \to \pi^+\pi^-)$ indicates a peripheral process and could be fitted by an exponential function $d\sigma/d|t| = d\sigma/d|t||_{t=0} \exp(-B\cdot|t|)$, B is given in Table 4 and in ref. [11]).
Taking these characteristics into account we used the following fit function in order to determine the fractions of ρ^0 and Δ production:

$$L = \sum_{i=1}^{N} g_i \ln \left\{ a_{\Delta^{++}} \frac{BW_\Delta e^{-B_\Delta|t_{\Delta^{++}}|}}{N_{\Delta^{++}}} + a_{\Delta^0} \frac{BW_\Delta e^{-B_\Delta|t_{\Delta^0}|}}{N_{\Delta^0}} + a_\rho \frac{BW_\rho \cdot W(\cos\theta_H,\phi_H) \cdot e^{-B_\rho|t_\rho|}}{N_\rho} + \frac{1 - a_\rho - a_{\Delta^{++}} - a_{\Delta^0}}{N_{PS}} \right\}$$

with N = number of events

g_i = weight of event

$a_{\Delta^{++}}, a_{\Delta^0}, a_\rho$ = fractions of $\Delta^{++}, \Delta^0, \rho$

$N_{\Delta^{++}}$ = normalisation integral (same for $N_{\Delta^0}, N_\rho, N_{PS}$)

$t_{\Delta^{++}}, t_{\Delta^0}, t_\rho$ = squared four-momentum transfers $p \to p\pi^+, p \to p\pi^-, \gamma \to \pi^+\pi^-$

For the $\Delta(1236)$ we use a shape which agrees with that expected from the πN phase shift δ_{33}:

$$BW_\Delta = \frac{\sin^2\delta_{33}}{\pi M_\Delta \Gamma(M_{p\pi})} \cdot \frac{M_{p\pi}}{\pi q(M_{p\pi})}$$

The values of δ_{33} have been taken from phase shift analysis[12]), further we use $q(M)$ = three momentum of the π^+ in the rest system of a $p\pi^+$ state with total mass M.

To take the ρ^0 mass shift[2,3,4,5,11]) into account (fig.8) we fitted the ρ^0 with two models:

i) <u>The "parametrization"</u> : The relativistic Breit-Wigner[13]) function is multiplied by $(M_\rho/M_{\pi\pi})^4$. This factor was proposed by Ross and Stodosky[14]) to account for the diffractive character of the ρ^0 production in the frame work of vector dominance.

$$BW_\rho = \frac{M_{\pi\pi}}{\pi q(M_{\pi\pi})} \cdot \frac{M_\rho \, \Gamma(M_{\pi\pi})}{(M_{\pi\pi}^2 - M_\rho^2)^2 + M_\rho^2 \Gamma^2(M_{\pi\pi})} \cdot \left(\frac{M_\rho}{M_{\pi\pi}}\right)^{n(t)}$$

$$\Gamma(M_{\pi\pi}) = \Gamma_\rho \left(\frac{q(M_{\pi\pi})}{q(M_\rho)}\right)^3 \cdot \frac{2}{1 + (q(M_{\pi\pi})/q(M_\rho))^2}$$

Instead of using an exponent of 4, the data are described more precisely if the exponent $n(t)$ is a free parameter depending on the squared four-momentum transfer t. The t-dependence of $n(t)$ could be described by the straight line fit

$$n(t) = (5.5 \pm 0.5) - (10.1 \pm 2.5)|t|.$$

For the mass and width we obtain the fitted values

$$M_\rho = (765.1 \pm 1.2)\text{MeV}, \quad \Gamma_\rho = (147.3 \pm 3.3)\text{MeV}.$$

ii) <u>The interference model</u>[15]): Here the ρ^0 mass shift is explained by an interference between a diffractively produced ρ^0 and a Drell type background. To avoid double counting a

rescattering term is added[16]).

In our fit BW_ρ is replaced by

$$BW_\rho = |F_\rho \hat{\varepsilon} \cdot \vec{q}(M_{\pi\pi}) + Y \cdot (F_{\pi^-} + F_{\pi^+})|^2$$

Y gives the relative amounts of the ρ^0 and the Drell term. F_ρ and F_π are the ρ and Drell amplitudes, respectively,

$$F_\rho = ie^{A_\rho \cdot t/2} (\sigma_\rho A_\rho e^{-A_\rho t_{min}})^{\frac{1}{2}} E_{cms} k_{cms} / (M^2 - M^2_{\pi\pi} - iM_\rho \Gamma)$$

$$F_{\pi^\pm} = \mp(\hat{\varepsilon}_0 \cdot \vec{q}_\pi) T(\pi^{\mp} p) G(t_{\pi^\pm}) / (m^2_\pi - t(\gamma \to \pi^\pm))$$

For G(t) we use the Ferrari-Selleri form factor[17]). For further details see ref.[3]).

The resonance fractions obtained must be corrected for events lost due to the veto counters. This is done examining the t-distributions in ρ^0 and Δ production. The corrections are typically 1% for the ρ^0 cross section and 18% for the Δ^{++} cross section.

The corrected cross sections are given in Table 5 and in figs. 10 and 11. The cross section given for Δ production is obtained using the "parametrization" for the ρ^0 production.

Some of the ρ^0 are produced in the backward direction in the center-of-mass system ($\cos\theta_{CMS} < 0$). Above $E_\gamma = 2.3$ GeV the effective mass for $\pi^+\pi^-$ shows for $\cos\theta_{CMS} < 0$ the f^0-meson at 1.270 GeV. To calculate the cross section for the f^0_{backw} production we use a hand drawn curve and correct the number of events for unobserved decay modes. The $\pi^+\pi^-$ effective mass and the cross sections for ρ^0 and f^0 production in backward direction are shown in fig. 12.

3.4. Resonance production in the channel $\gamma p \to p\pi^+\pi^-\pi^0$

In figs. 13-15 we show $M_{\pi^+\pi^-\pi^0}$, $M_{\pi^+\pi^-}$, $M_{\pi^+\pi^0}$, $M_{\pi^-\pi^0}$, $M_{p\pi^+}$, $M_{p\pi^-}$ effective mass distributions of the reaction $\gamma p \to p\pi^+\pi^-\pi^0$. These distributions are not corrected for events in which the proton is stopped inside the target (giving a two-prong unfitted event) or where one particle has an angle $\theta < 2^\circ$ with respect to the beam axis.

Consequently the ω peak looks smaller at medium energies than at higher energies, due to the different thicknesses of the target counter.

The ω production cross section is obtained by interpolating the background from below and above the peak mass region. The corrections for acceptance losses are of the order of 15%-30% at different energies. The results are given in Table 6 and fig.16 where an additional correction for unobserved ω decay modes has been applied. In addition the cross section for backward produced ω ($\cos\theta_{CMS} < 0$) is given (fig.17).

The η signal is free from background. The η production cross section was corrected for acceptance losses and unseen decays of the η.

Besides the reactions $\gamma p \to p\omega$ and $\gamma p \to p\eta$, we further observed inelastic production of $\rho^+,\rho^0,\rho^-,\Delta^+,\Delta^{++}$ and double resonance production of $\Delta^{++}\rho^-$ and $\Delta^+\rho^0$.

To determine the cross sections for ρ,Δ and $\rho\Delta$ production we use the Maximum Likelihood fit function

$$L = \sum_1^N g_i \ln \left\{ \sum_\rho a_\rho \left(\frac{BW_\rho}{N_\rho}\right) + \sum_\Delta a_\Delta \left(\frac{BW_\Delta}{N_\Delta}\right) + \sum_{\Delta\rho} a_{\Delta\rho} \left(\frac{BW_{\Delta\rho}}{N_{\Delta\rho}}\right) + \left(1 - \sum_{\rho,\Delta,\Delta\rho} a_i\right) \frac{1}{N_{PS}} \cdot f(t) \right\}$$

where $\rho = \rho^+,\rho^-,\rho^0$, $\Delta = \Delta^{++},\Delta^+,\Delta^0$.

In the fit we use only events outside the ω region ($M_{\pi\pi\pi} > 0.88$ GeV). $f(t)$ describes the t-distribution of the background and is taken to be $f(t) = \frac{1}{(t-m_\pi^2)}$.

BW_ρ is the relativistic Breit-Wigner function as described in section 3.3 without the factor $(M_\rho/M_{\pi\pi})^4$, and $BW_{\Delta\rho} = BW_\Delta \cdot BW_\rho$. For these reactions the corrections for acceptance losses are negligible.

The results are summarized in Table 6 and fig.16.

3.5. Resonance production in the channel $\gamma p \to n2\pi^+\pi^-$

We show in figs. 18 and 19 the distributions of the effective masses $M_{\pi^+\pi^-}$, $M_{n\pi^-}$ and $M_{\pi^+\pi^+\pi^-}$ for the reaction $\gamma p \to n\pi^+\pi^+\pi^-$. This channel is dominated by production of Δ^- and ρ^0 while production of Δ^+ and the two-body reaction $\gamma p \to \Delta^+\rho^0$ are unimportant. We use the same fit procedure as described in the previous section. To take the two combinations for the ρ^0 into account we add the fitted fractions for each combination.

In the photon energy region above $E_\gamma > 3.25$ GeV we find a small signal for production of the A_2^+. In order to get the fraction of A_2^+ we include a term $a_A \cdot (1/t_{p\to n}) \cdot BW_A(\pi^+\pi^+\pi^-)/N_A$ into our fit function. At lower energies the phase space has its maximum near the A_2 mass inhibiting any A_2 separation.

The cross sections are given in Table 7.

3.6. Resonance production in the channel $\gamma p \to p2\pi^+2\pi^-$

In this channel we consider only ρ^0, Δ^{++} and some A_2^- production (fig.20). To take the four combinations of $\pi^+\pi^-$ for the ρ into account, and to avoid confusion with the sum of all fractions a_i being less than one we chose the following likelihood function:

$$L = \sum_{i=1}^{N} g_i \ln\left\{ \sum_{p=1}^{N_{comb}} \left(\sum_{i=1}^{N_{ch}} C_i \frac{BW\ f(t)}{N} \right) + \frac{1 - \Sigma\ C_i}{N_{PS}} \right\}$$

The first sum in the brackets is for the combinations, the second one for the different reactions (ρ, Δ, A_2). The fractions a_i are then given by $a_i = N_{comb} * C_i$.

For f(t) we use an exponential function $\exp(-b|t|)$ where b is fitted; the results for b, averaged over the whole energy range, are $b = 2.3 \pm 0.5$ for ρ^0, $b = 1.2 \pm 0.3$ for Δ^{++} and $b = 1.2 \pm 0.3$ for A_2^- production.

The resulting cross sections are shown in fig.21 and Table 8.

3.7. Resonance production in the channel $\gamma p \to p 2\pi^+ 2\pi^- \pi^0$

The mass distributions of this channel show evidence for ω, η, X^0, ρ^0 and Δ^{++} production (fig.22). To calculate the fractions we use the fit procedure described in the previous chapter. For the shape of the ω and η a Gaussian $G = \exp(-(m-m_0)^2/2\sigma_0^2)$ is used.

The widths were characterized by the mass resolution $\sigma_0 = 20$ MeV of our experiment.

To determine a production cross section for the X^0 we plot the $\eta\pi^+\pi^-$ mass using all η events. In this distribution the X^0 shows up as a peak above the background. The cross sections, for ω, η and X^0 production corrected for unobserved decay modes, are given in fig.23 and Table 8.

3.8. Resonance production in the channel $\gamma p \to n 3\pi^+ 2\pi^-$

The only significant resonance signal observed in the mass distributions of this channel is the Δ^- (fig.24). The cross section is determined with the fit described in chapter 3.6 and given in Table 8.

3.9 Resonance production in the channel $\gamma p \to p\pi^+\pi^-$ (+ neutrals)

In this section we want to look for resonance production in the $\pi^+\pi^-(m\pi^0)$ final state with $m \geq 2$ where perhaps the $B^0 \to \omega\pi^0 \to \pi^+\pi^- 2\pi^0$ should give a peak at 1.235 GeV. In 40 % of the nofit events with three charged outgoing tracks we can distinguish by ionization between events which have a proton or a neutron in the final state but of course we know neither the number of π^0 nor their momenta. In fig. 25a we show the invariant mass for events with $|t_{p\to p}| < 0.5$ (GeV/c)^2 and 0.34 GeV $< M_{\pi^+\pi^-} <$ 0.58 GeV which is the average mass of the two π's from the ω decay. Because the phasespace for events with $E_\gamma < 4.0$ GeV has its maximum near the expected B^0-mass we use only the high energy data with $E_\gamma \geq 4.0$ GeV. In fig. 25a one can see an enhancement at 1240 MeV. Monte Carlo events exclude that the peak at 1240 MeV is perhaps a reflection of Δ, ρ or ω production. In fig. 25b the Δ is removed by a cut in the $p\pi^+$ mass. Interpreting the peak at 1240 MeV as a B^0 we obtain a cross section of

$$\sigma(\gamma p \to pB^0 \to p\pi^+\pi^- 2\pi^0) = 0.5 \pm 0.2\ \mu b$$

for 4.0 GeV $< E_\gamma <$ 6.3 GeV.

Conclusion

In this experiment we examined the photoproduction on hydrogen over a wide photon energy range (1.6-6.3 GeV). An energy tagged photon beam and a nearly 4π trigger on hadronic events in a streamer chamber allowed for recording single interactions and assigning to them the photon energy within 1%. With measured accuracies comparable to those of previous photoproduction experiments with optical detectors we analysed all exclusive final states comprised of 3,5,7 charged particles with or without one neutral particle.
We report the energy dependence of topological and reaction cross sections. All reactions exhibit substantial resonance productions, and in particular ρ and $\Delta(1236)$. We applied Maximum-Likelihood fits to most of the reactions. The resonance production cross sections obtained are listed. Those cross sections which are also measured by previous experiments agree within errors with the published data.

Acknowledgements

We wish to thank Professors M.Deutschmann, E.Lohrmann, N.Schmitz and M.W.Teucher for their steady encouragement throughout the experiment. We are indebted to Dr. P. Söding for critical assistance in the analysis of the data. We thank Drs. G.Horlitz and S.Wolff and their crew for their steady support. The technical assistance of H.J.Gebauer, Miss E.Hell, Mrs. B.Hentschel, H.Hildebrandt, K.Klinkmüller, G.Kraft, Mrs. C.Ponting, H.Sabath, H.Sass, K.Westphal and K.H.Wroblewski is gratefully acknowledged. We thank our scanning teams for their careful work. We would like to thank the DESY synchrotron group and the Hallendienst for their excellent machine performance.

Financial support was given by the Bundesministerium für Forschung und Technologie.

REFERENCES

1) Cambridge Bubble Chamber Group, Phys. Rev. 146(1966)994, 155(1967)1468, 163,(1967)1510, 160(1969)1081.

2) Aachen-Berlin-Bonn-Hamburg-Heidelberg-München Collaboration, Phys. Rev. 175(1968)1669, 188(1969)2060.

H. Spitzer, Internal report, DESY F1-71/4(1971).

3) SLAC-Berkeley-Tufts Collaboration, Phys. Rev. Letters 23 (1969)498, 24(1970)955, 24(1970)960, 24(1970)1467(E), 24(1970)1364, 25(1970)1223, Nucl. Phys. B29(1971)349, Phys. Rev. D5(1973)3150, Phys. Rev. D5(1972)545.

4) M. Davier et al., Phys. Rev. Letters 20(1968)952, 21(1968)841, Phys. Letters 28B(1969)619, Phys. Rev. D1(1970)790, Nucl. Phys. B36(1972)404, Nucl.Phys B81(1974)205

5) SLAC-Weizmann-Tel Aviv Collaboration, Phys. Rev. Letters 22(1969)669, 23(1969)1322, 25(1970)764, Nucl. Phys. B25(1971)499, Phys. Rev. D5(1972)15.

6) V. Eckardt and A. Ladage, Proc. of the Int. Conf. on Instrumentation for High Energy Physics, Dubna 1970;

V. Eckardt, University of Hamburg, thesis (1972).

7) CERN TC-Library.

8) F. Selonke, University of Bonn, thesis (1973). DESY R2-73/2;

H.J. Mück, University of Bonn, thesis (1972). DESY R2-72/1.

9) D.O. Caldwell et al., Phys. Rev. Letters 25(1970)609, 902(E);

H. Meyer et al., Phys. Letters 33B(1970)189;

H.G. Hilpert et al., Phys. Letters 27B(1968)474.

10) G. Wolf, in Proceedings of the International Symposium on Electron and Photon Interactions at High Energies, Cornell University, Ithaca, N.Y., 1971.

11) Aachen-Hamburg-Heidelberg-München Collaboration, Nucl. Phys. B47(1972)436, B57(1973)1.

12) A. Donnachie, R.C. Kirsopp, C. Lovelace, CERN Report No. TH 838(1967) (unpublished).

13) K. Gottfried, J.D. Jackson, Nuovo Cimento 33(1964)309.

14) M. Ross and L. Stodolsky, Phys. Rev. 149(1966)1172.

15) P. Söding, Phys. Letters 19(1965)702.

16) T. Bauer, Phys. Rev. Letters 25(1970)485;

J. Pumplin, Phys. Rev. D2(1970)1859.

17) E. Ferrari, F. Selleri, Phys. Rev. Letters 7(1961)387.

18) W.J. Podolsky, Thesis, Berkeley UCRL-20128(1971), unpublished.

19) D. Lüke, University of Hamburg, thesis (1972).

Table captions

1. Corrections and systematic uncertainties for calculating the topological cross sections.
2. Topological cross sections (μb).
   The cross sections for events with visible strange particles are not included in the prong cross sections. It should be noted that these cross sections are experiment-dependent.
3. Channel cross sections (μb) of reactions with 3,5 and 7 outgoing tracks.
4. Reaction $\gamma p \to p\rho^0$
   Parameters of the differential cross sections

$$\frac{d\sigma}{d|t|} = \left.\frac{d\sigma}{d|t|}\right|_{t=0} \cdot \exp(-B|t|)$$

5. Reaction cross sections (μb) of the channel $\gamma p \to p\pi^+\pi^-$.
6. Cross sections of the channel $\gamma p \to p\pi^+\pi^-\pi^0$ (μb).
   Quasi-two-body reactions are not included in the other corresponding reactions.
7. Cross sections of the channel $\gamma p \to n2\pi^+\pi^-$ (μb).
8. Cross sections of the channels $\gamma p \to p2\pi^+2\pi^-$, $\gamma p \to p2\pi^+2\pi^-\pi^0$ and $\gamma p \to n3\pi^+2\pi^-$ (μb).
   Quasi-two-body reactions are not included in the other corresponding reactions.

Scanning and measuring of events with total charge on outgoing visible tracks Q = 0 or 1 only	3±1%
Scanning losses	±1%
Veto weight for events with tracks having $\theta > 2^{\circ}$	16±2%
" " " " " " " $\theta < 2^{\circ}$	2±2%
Inefficiency of target counter for $E_{\gamma} > 4.0$ GeV and two prong events	46±5%
Inefficiency of target counter for $E_{\gamma} > 4.0$ GeV and events with more than two tracks	10±2%

Table 1

Corrections and systematic uncertainties for calculating the topological cross section.

Topological cross section σ(μb)

Beam energy E_γ (GeV)	1.6-1.9	1.9-2.1	2.1-2.3	2.3-2.6	2.6-3.25	3.25-4.0	4.0-5.0	5.0-6.3
3 prong	93.5±3.8	95.1±4.0	97.1±4.3	94.1±3.2	92.8±3.1	87.1±3.6	78.2±5.0	73.4±5.3
5 prong	3.3±0.5	3.6±0.5	3.2±0.5	6.4±0.5	10.0±0.7	14.0±1.1	20.6±1.3	25.5±1.6
7 prong	—	—	—	0.1±0.1	0.2±0.1	0.6±0.2	1.1±0.2	2.1±0.3
with visible strange particle decay	5.2±0.6	5.9±0.7	5.9±0.7	6.9±0.6	6.5±0.5	9.1±0.8	8.4±0.8	8.7±0.9

Table 2

Channel Cross Sections (μb)

Table 3

Beam energy E_γ (GeV)	1.6-1.9	1.9-2.1	2.1-2.3	2.3-2.6	2.6-3.25	3.25-4.0	4.0-5.0	5.0-6.3
3 prongs								
$p\pi^+\pi^-$	41.7±2.3	39.7±2.4	38.5±2.4	33.8±1.7	28.1±1.6	23.4±1.2	22.5±2.0	19.5±1.8
$p\pi^+\pi^-\pi^0$	25.9±1.7	25.0±1.8	26.0±2.1	23.6±1.3	23.2±1.3	18.8±1.4	18.0±1.6	14.4±1.5
$n2\pi^+\pi^-$	8.0±0.8	11.4±1.1	9.1±1.0	9.5±0.7	11.3±0.8	9.8±0.9	7.9±1.3	7.7±1.3
$p\pi^+\pi^-(\geq 2\pi^0)$ $n2\pi^+\pi^-(\geq 1\pi^0)$	17.9±1.1	19.0±1.3	23.6±1.7	27.2±1.3	30.2±1.4	35.0±1.9	29.8±2.3	31.8±2.4
5 prongs								
$p2\pi^+2\pi^-$	3.0±1.0	2.9±0.8	2.0±0.6	3.4±0.6	4.5±0.6	4.4±0.5	5.5±0.5	5.4±0.4
$p2\pi^+2\pi^-\pi^0$	—	0.3±0.2	0.6±0.2	1.4±0.3	2.7±0.5	4.0±0.5	5.7±0.6	7.4±0.6
$n3\pi^+2\pi^-$	—	0.1±0.1	0.2±0.2	0.3±0.1	0.5±0.2	1.5±0.3	2.3±0.3	2.2±0.3
$p2\pi^+2\pi^-(\geq 2\pi^0)$ $n3\pi^+2\pi^-(\geq 1\pi^0)$	0.3±0.3	0.3±0.2	0.4±0.2	1.3±0.4	2.3±0.5	4.1±0.6	7.1±0.9	10.5±1.1
7 prongs								
$p3\pi^+3\pi^-$	—	—	—	—	0.1±0.1	0.3±0.1	0.5±0.1	0.5±0.1
$p3\pi^+3\pi^-\pi^0$	—	—	—	—	—	0.1±0.1	0.4±0.1	0.7±0.2
$n4\pi^+3\pi^-$	—	—	—	—	—	—	0.1±0.1	0.2±0.1
$p3\pi^+3\pi^-(\geq 2\pi^0)$ $n4\pi^+3\pi^-(\geq 1\pi^0)$	—	—	—	0.1±0.1	0.1±0.1	0.1±0.1	0.1±0.1	0.7±0.2

Beam energy E_γ (GeV)	"Parametrization"		Interference model	
	$\left.\frac{d\sigma}{d\|t\|}\right\|_{t=0}$ $\frac{\mu b}{(GeV/c)^2}$	B $(GeV/c)^{-2}$	$\left.\frac{d\sigma}{d\|t\|}\right\|_{t=0}$ $\frac{\mu b}{(GeV/c)^2}$	B $(GeV/c)^{-2}$
1.6-2.1	205±20	7.8±0.4	143±17	6.1±0.4
2.1-2.6	160±13	6.9±0.3	135±14	5.8±0.3
2.6-3.25	134±9	7.6±0.3	105±9	5.8±0.3
3.25-4.0	128±9	8.1±0.3	112±10	5.7±0.3
4.0-6.3	158±13	8.9±0.4	135±19	8.0±0.5

Reaction $\gamma p \to p\rho^0$,

Parameters of the differential cross section

$$\frac{d\sigma}{d|t|} = \left.\frac{d\sigma}{d|t|}\right|_{t=0} \cdot \exp(-B \cdot |t|)$$

Table 4

Reaction Cross Sections (μb)

Channel $\gamma p \to p\pi^+\pi^-$

Reaction \ Beam energy E_γ (GeV)	1.6-1.9	1.9-2.1	2.1-2.3	2.3-2.6	2.6-3.25	3.25-4.0	4.0-5.0	5.0-6.3
$p\rho^o$ parametrisation	21.8 ± 1.4	22.1 ± 1.7	22.2 ± 1.6	19.7 ± 1.1	18.5 ± 1.1	17.7 ± 1.0	18.9 ± 2.0	17.4 ± 2.0
$p\rho^o$ interference model	19.2 ± 1.6	20.7 ± 1.9	20.8 ± 1.8	17.0 ± 1.3	17.0 ± 1.3	17.0 ± 1.2	15.2 ± 1.4	
$p\rho^o$ backw ($\cos\theta < 0$)	2.8 ± 0.8	1.1 ± 0.5	0.8 ± 0.7	0.7 ± 0.2	0.5 ± 0.2	0.2 ± 0.1	0.1 ± 0.1	0.1 ± 0.1
pf^o * backw ($\cos\theta < 0$)	-	-	-	1.3 ±0.37	0.39±0.13	0.19 ± 0.06	0.1 ± 0.1	
$\Delta^{++}\pi^-$	6.1 ± 1.0	5.4 ± 0.9	4.2 ± 0.8	3.8 ± 0.6	2.9 ± 0.5	1.7 ± 0.5	1.2 ± 0.2	0.9 ± 0.2
$\Delta^o (\to p\pi^-)\pi^+$	0.9 ± 0.6	0.7 ± 0.7	0.2 ± 0.5	0.1 ± 0.2	0.2 ± 0.2	0.1 ± 0.2	0.4 ± 0.1	0.3 ± 0.1

* corrected for unobserved decay modes

Table 5

Reaction Cross Sections (μb)

Channel $\gamma p \to p\pi^+\pi^-\pi^0$

Reaction \ Beam energy E_γ(GeV)	1.6-2.1	2.1-2.6	2.6-3.25	3.25-4.0	4.0-5.0	5.0-6.3
$p\omega^*$	7.6±1.5	5.3±0.5	3.9±0.3	1.8±0.2	2.7±0.5	2.0±0.5
$p\omega^*_{backw}$ ($\cos\theta < 0$)	2.1±0.5	0.8±0.1	0.13±0.04	0.14±0.05	0.13±0.04	
$p\eta^*$	0.6±0.4	0.3±0.2	0.1±0.1	0.1±0.1	0.2±0.1	
$p\rho^0\pi^0$	1.1±0.4	1.1±0.4	1.0±0.3	0.3±0.3	0.2±0.3	0.0±0.3
$p\rho^+\pi^-$	1.8±0.5	2.0±0.4	2.2±0.4	1.8±0.4	1.2±0.4	1.3±0.3
$p\rho^-\pi^+$	0.8±0.5	1.9±0.5	1.7±0.4	0.7±0.3	0.8±0.4	0.9±0.3
$\Delta^{++}\pi^-\pi^0$	0.5±0.3	0.8±0.5	1.2±0.3	0.8±0.3	0.4±0.2	0.3±0.2
$\Delta^+(\to p\pi^0)\pi^+\pi^-$	0.4±0.3	1.2±0.5	1.1±0.3	0.8±0.3	0.0±0.2	0.1±0.2
$\Delta^{++}\rho^-$	3.5±0.6	2.8±0.5	0.9±0.4	0.5±0.2	0.4±0.2	0.5±0.2
$\Delta^+(\to p\pi^0)\rho^0$	0.3±0.5	0.4±0.4	0.0±0.3	0.0±0.2	0.7±0.2	0.6±0.2

* Corrected for decays other than $\pi^+\pi^-\pi^0$

Table 6

Reaction Cross Sections (μb)

Channel $\gamma p \to n2\pi^+\pi^-$

Reaction \ Beam energy E_γ (GeV)	1.6-2.1	2.1-2.6	2.6-3.25	3.25-4.0	4.0-5.0	5.0-6.3
$n\rho^0\pi^+$	0.06±0.05	1.54±0.15	1.32±0.25	0.84±0.24	0.71±0.4	0.95±0.45
$\Delta^+(\to n\pi^+)\pi^+\pi^-$	0.02±0.05	0±0.05	0±0.05	0±0.05	0±0.2	
$\Delta^-\pi^+\pi^+$	2.13±0.40	1.60±0.25	1.17±0.30	0.67±0.16	0.24±0.2	0.15±0.15
$\Delta^+(\to n\pi^+)\rho^0$	0.02±0.05	0.25±0.10	0.16±0.10	0.21±0.10	0.2±0.2	
nA_2^{+*}	—	—	—	0.7 ±0.3	0.3±0.3	

* corrected for decays other than $\pi^+\pi^-\pi^0$

Table 7

Reaction cross sections (μb)

Reaction \ Beam energy E_γ (GeV)	2.1-2.6	2.6-3.25	3.25-4.0	4.0-5.0	5.0-6.0
$\gamma p \to p2\pi^+2\pi^-$					
$p\rho^0\pi^+\pi^-$	0.3±0.3	1.4±0.6	2.0±0.7	3.1±0.8	3.3±0.8
$\Delta^{++}\pi^+2\pi^-$	1.9±0.5	1.1±0.5	0.9±0.4	1.5±0.3	0.7±0.2
$\Delta^{++}A_2^-$	—	—	—	0.5±0.2	
$\Delta^{++}\rho^0\pi^-$	—	0.3±0.2		0.3±0.2	
$\gamma p \to p2\pi^+2\pi^-\pi^0$					
$p\pi^+\pi^-\omega^*$	0.5±0.2	1.8±0.3	2.0±0.3	1.6±0.2	
$p\pi^+\pi^-\eta^*$	1.4±0.3	2.8±0.4	1.0±0.3	1.1±0.4	
pX^0	0.3±0.15	0.3±0.15	0.3±0.1	0.2±0.1	
$p\rho^0\pi^+\pi^-\pi^0$	—	—	0.8±0.2	1.1±0.3	
$\Delta^{++}\pi^+2\pi^-\pi^0$	1.0±0.2			1.3±0.3	
$\gamma p \to n3\pi^+2\pi^-$					
$\Delta^-3\pi^+\pi^-$	0.4±0.2			0.5±0.2	

Table 8

Figure captions.

1 : Experimental setup - Tagging system.

2 : Experimental setup - Streamer chamber and Trigger counters.

3 : Energy dependence of the topological cross sections. All cross sections except the total - 1-prong cross section are normalized to expression (1) given in section 2.5 (dashed line). E_γ is the photon energy in the laboratory system.

4 : Energy dependence of the total cross section for the reaction $\gamma p \to p\pi^+\pi^-$.

5 : Energy dependence of the total cross sections for the reactions $\gamma p \to p\pi^+\pi^-\pi^0$ and $\gamma p \to n\pi^+\pi^+\pi^-$.

6 : Energy dependence of the total cross sections for the reactions $\gamma p \to p2\pi^+2\pi^-$, $\gamma p \to p2\pi^+2\pi^-\pi^0$ and $\gamma p \to n3\pi^+2\pi^-$.

7 : Energy dependence of the total cross sections for the reactions $\gamma p \to p3\pi^+3\pi^-$, $\gamma p \to p3\pi^+3\pi^-\pi^0$ and $\gamma p \to n4\pi^+3\pi^-$.

8 : Reaction $\gamma p \to p\pi^+\pi^-$. Distribution of the effective mass $M_{\pi^+\pi^-}$ for a) $1.6\text{GeV}<E_\gamma<2.6\text{GeV}$, b) $2.6\text{GeV}<E_\gamma<4.0\text{GeV}$ and c) $4.0\text{GeV}<E_\gamma<6.3\text{GeV}$.*

9 : Reaction $\gamma p \to p\pi^+\pi^-$. Distribution of the effective mass $M_{p\pi^+}$ for a) $1.6\text{GeV}<E_\gamma<2.6\text{GeV}$, b) $2.6\text{GeV}<E_\gamma<4.0$ GeV and c) $4.0\text{GeV}<E_\gamma<6.3\text{GeV}$.*

10 : Energy dependence of the cross section for the reaction $\gamma p \to p\rho^0$, using fit (i) (see 3.3).

11 : Energy dependence of the cross section for the reactions $\gamma p \to \Delta^{++}\pi^-$ and $\gamma p \to \Delta^0\pi^+$.

12 : Distribution of the effective mass $M_{\pi^+\pi^-}$ for $2.3 \leq E_\gamma \leq 3.25$ and $\cos\theta^* < 0$ and energy dependence of the cross sections for backward produced ρ^0 and f^0.

13 : Reaction $\gamma p \to p\pi^+\pi^-\pi^0$. Distribution of the effective masses $M_{\pi^+\pi^-\pi^0}$ and $M_{\pi^+\pi^-}$ for a) $1.6\text{GeV}<E_\gamma<2.6\text{GeV}$, b) $2.6\text{GeV}<E_\gamma<4.0\text{GeV}$ and c) $4.0\text{GeV}<E_\gamma<6.3\text{GeV}$.*

14 : Reaction $\gamma p \to p\pi^+\pi^-\pi^0$. Distribution of the effective masses $M_{\pi^+\pi^0}$ and $M_{\pi^-\pi^0}$ for a) $1.6\text{GeV}<E_\gamma<2.6\text{GeV}$, b) $2.6\text{GeV}<E_\gamma<4.0\text{GeV}$ and c) $4.0\text{GeV}<E_\gamma<6.3\text{GeV}$.*

15 : Reaction $\gamma p \to p\pi^+\pi^-\pi^0$. Distribution of the effective masses $M_{p\pi^+}$ and $M_{p\pi^0}$ for a) $1.6\text{GeV}<E_\gamma<2.6\text{GeV}$, b) $2.6\text{GeV}<E_\gamma<4.0\text{GeV}$ and c) $4.0\text{GeV}<E_\gamma<6.3\text{GeV}$.*

---

* Not corrected for "total losses" (see 3.1).

16 : Energy dependence of the cross sections for the reactions $\gamma p \to p\omega$, $\gamma p \to p\rho^0\pi^0$, $\gamma p \to p\rho^+\pi^-$, $\gamma p \to p\rho^-\pi^+$ and $\gamma p \to \Delta^{++}\rho^-$. The SBT-Data for the reactions with ρ or Δ were taken from ref.[18].

17 : Energy dependence of the cross section for backward produced ω ($\cos\theta_{CMS}<0$) in the reaction $\gamma p \to p\omega$.

18 : Reaction $\gamma p \to n2\pi^+\pi^-$. Distribution of the effective masses $M_{\pi^+\pi^-}$ and $M_{n\pi^-}$ for a) $1.6\text{GeV}<E_\gamma<2.6\text{GeV}$, b) $2.6\text{GeV}<E_\gamma<4.0\text{GeV}$ and c) $4.0\text{GeV}<E_\gamma<6.3\text{GeV}$.*

19 : Reaction $\gamma p \to n2\pi^+\pi^-$. Distribution of the effective mass $M_{\pi^+\pi^+\pi^-}$ for a) $1.6\text{GeV}<E_\gamma<2.6\text{GeV}$ b) $2.6\text{GeV}<E_\gamma<4.0\text{GeV}$ and c) $4.0\text{GeV}<E_\gamma<6.3\text{GeV}$.*

20 : Reaction $\gamma p \to p2\pi^+2\pi^-$. Distribution of the effective masses $M_{\pi^+\pi^-}$, $M_{p\pi^+}$ and $M_{\pi^+\pi^+\pi^-\pi^-}$ for a) $1.6\text{GeV}<E_\gamma<4.0\text{GeV}$ and b) $4.0\text{GeV}<E_\gamma<6.3\text{GeV}$.*

21 : Energy dependence of the reactions $\gamma p \to p\pi^+\pi^-\rho^0$ and $\gamma p \to \Delta^{++}\pi^+2\pi^-$.

22 : Reaction $\gamma p \to p2\pi^+2\pi^-\pi^0$. Distribution of the effective masses $M_{\pi^+\pi^-}$, $M_{p\pi^+}$, $M_{\pi^+\pi^-\pi^0}$ and $M_{\pi^+\pi^+\pi^-\pi^-\pi^0}$ (with $M_{\pi^+\pi^-\pi^0} < 0.6$ GeV) for a) $1.6\text{ GeV} < E_\gamma < 4.0$ GeV and b) $4.0\text{ GeV} < E_\gamma < 6.3$ GeV.*

23 : Energy dependence of the cross sections for the reactions $\gamma p \to p\pi^+\pi^-\omega$, $\gamma p \to p\pi^+\pi^-\eta$ and $\gamma p \to p\eta'$.

24 : Reaction $\gamma p \to n3\pi^+2\pi^-$. Distribution of the effective mass $M_{n\pi^-}$ for a) $1.6\text{GeV}<E_\gamma<4.0\text{GeV}$ and b) $4.0\text{GeV}<E_\gamma<6.3\text{GeV}$.*

25 : a) Reaction $\gamma p \to p\pi^+\pi^-(m\pi^0)$, $m \geq 2$. Mass recoiling from proton with $|t| < 0.5$ (GeV/c)^2 with selection of $0.34\text{ GeV} < M_{\pi^+\pi^-} < 0.58$ GeV to enhance events with $\pi^+\pi^-$ from ω decay. b) The Δ's are removed by a $M_{p\pi^+} > 1.32$ GeV cut.

---

* Not corrected for "total losses" (see 3.1).

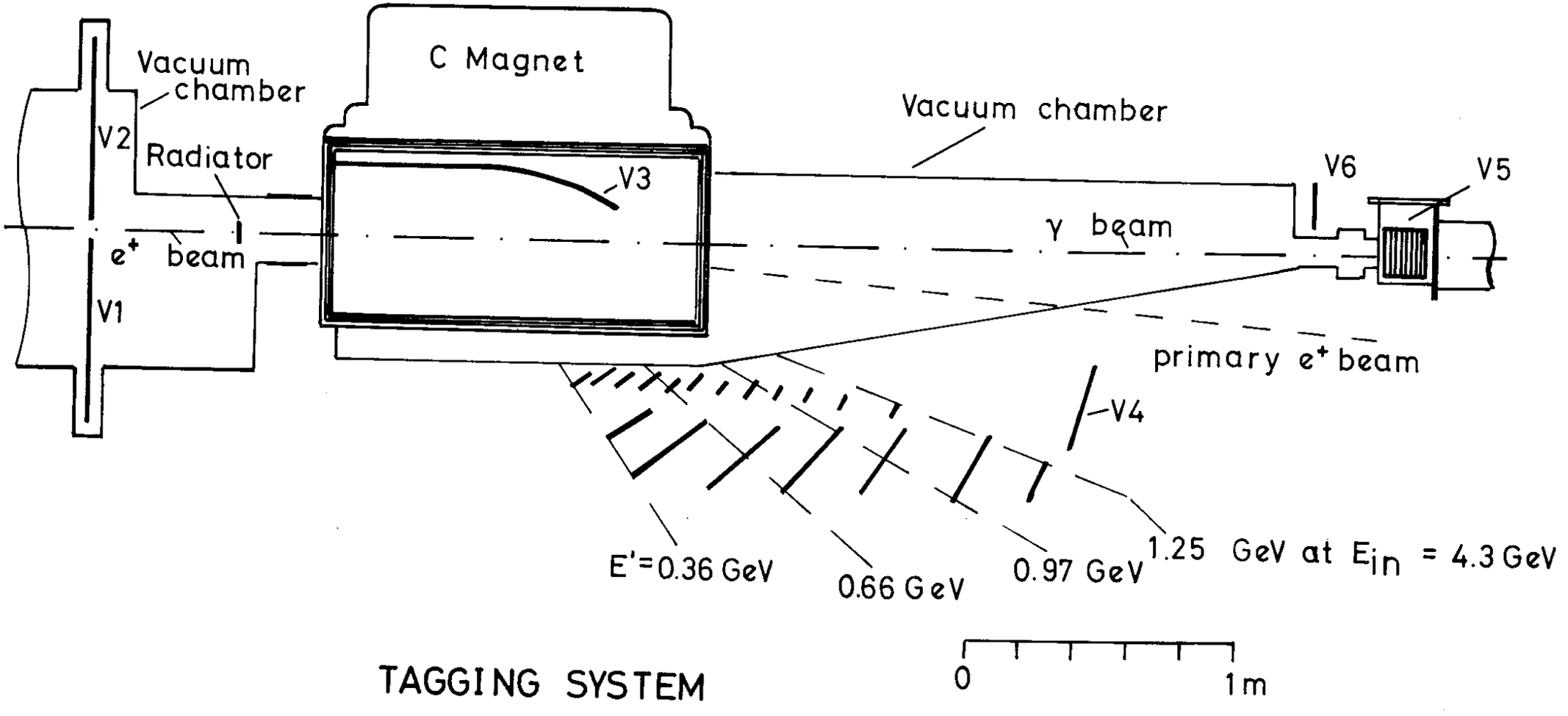
Vacuum chamber
C Magnet
Vacuum chamber
V2
Radiator
V3
V6
V5
γ beam
e+ beam
V1
primary e+ beam
V4
E'=0.36 GeV
0.66 GeV
0.97 GeV
1.25 GeV at Ein = 4.3 GeV
0
1m
TAGGING SYSTEM

Fig. 1

EXPERIMENTAL SETUP

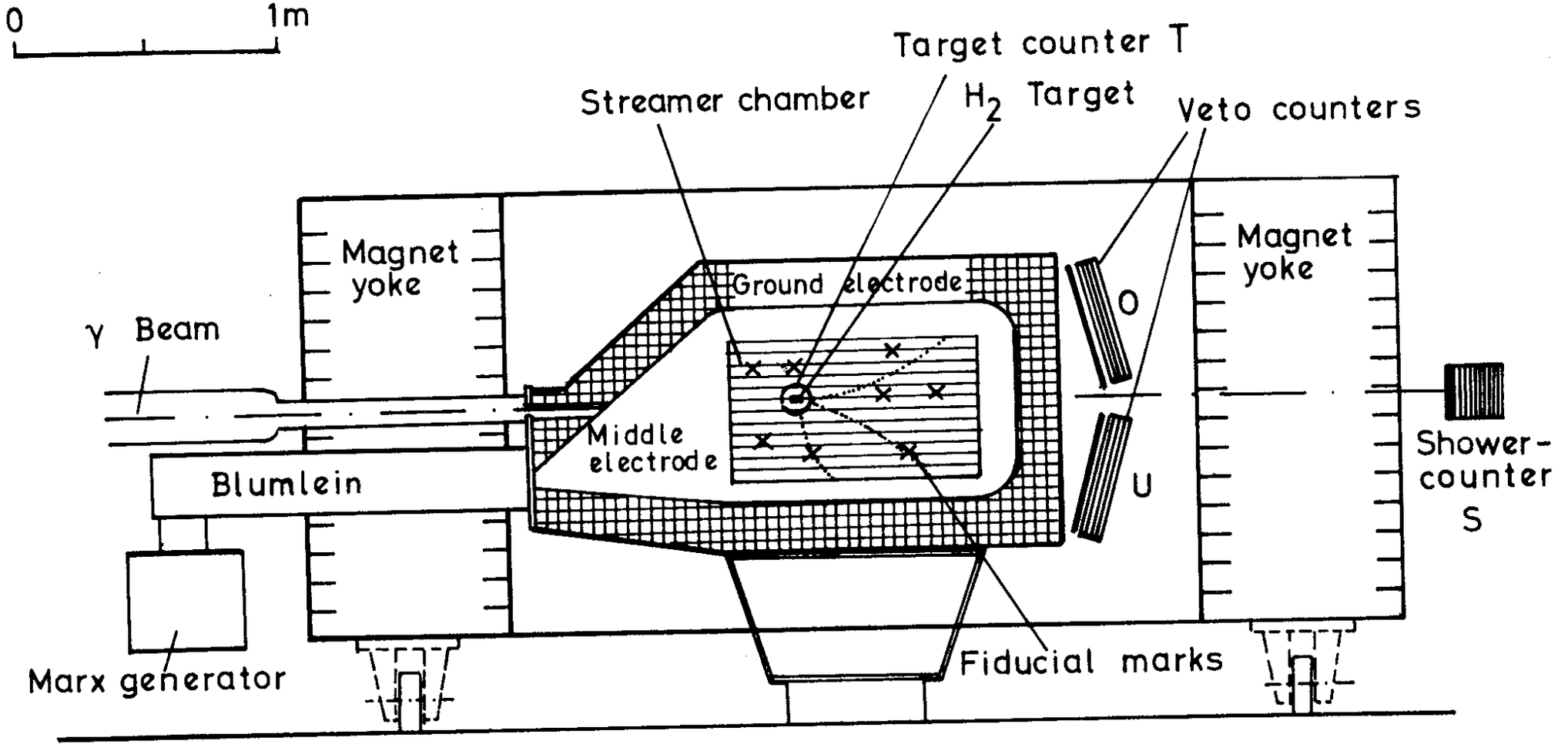

Fig. 2

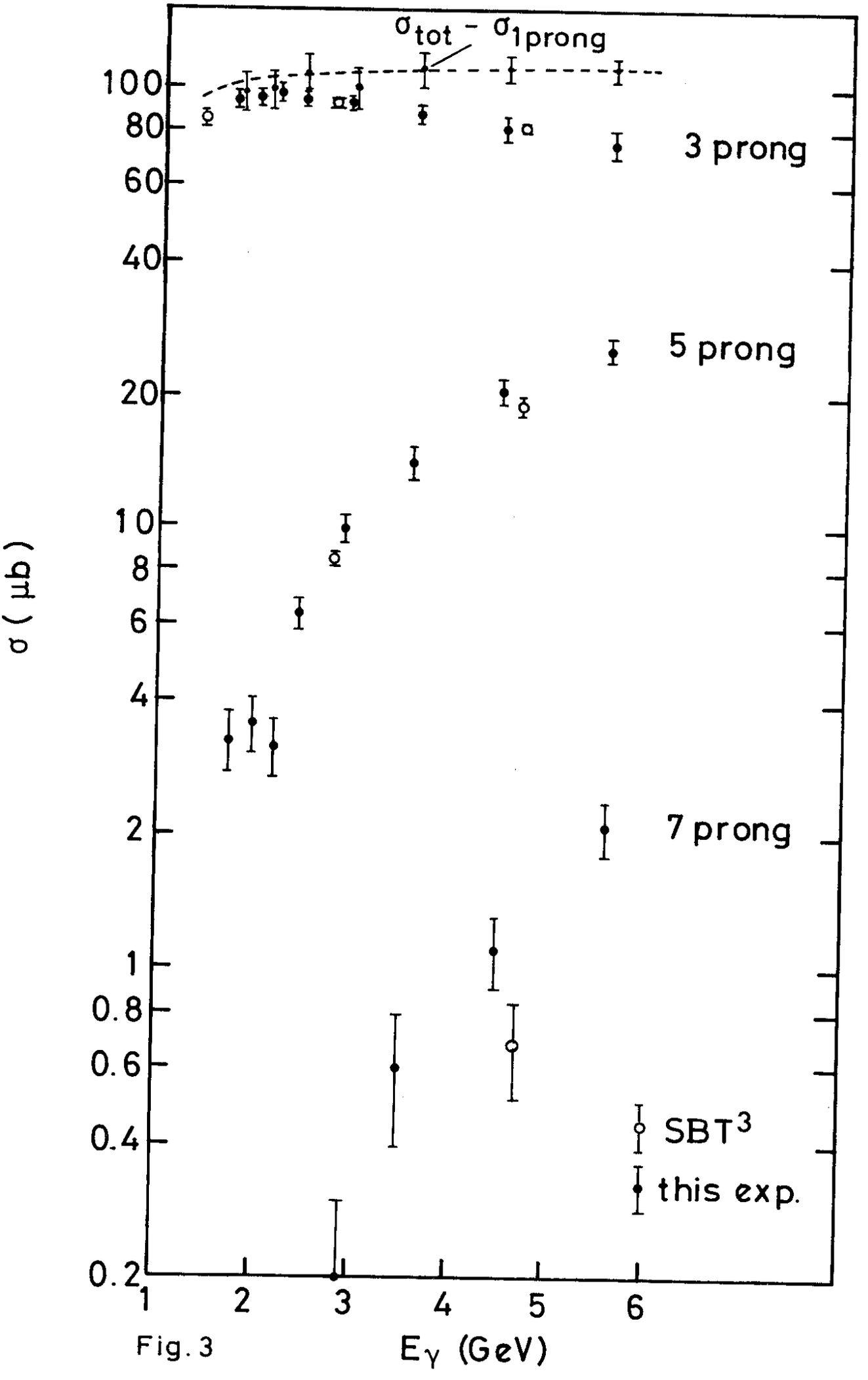
$\sigma_{tot} - \sigma_{1prong}$
3 prong
5 prong
7 prong
SBT[3]
this exp.
σ (μb)
E_γ (GeV)
100
80
60
40
20
10
8
6
4
2
1
0.8
0.6
0.4
0.2
1
2
3
4
5
6

Fig. 3

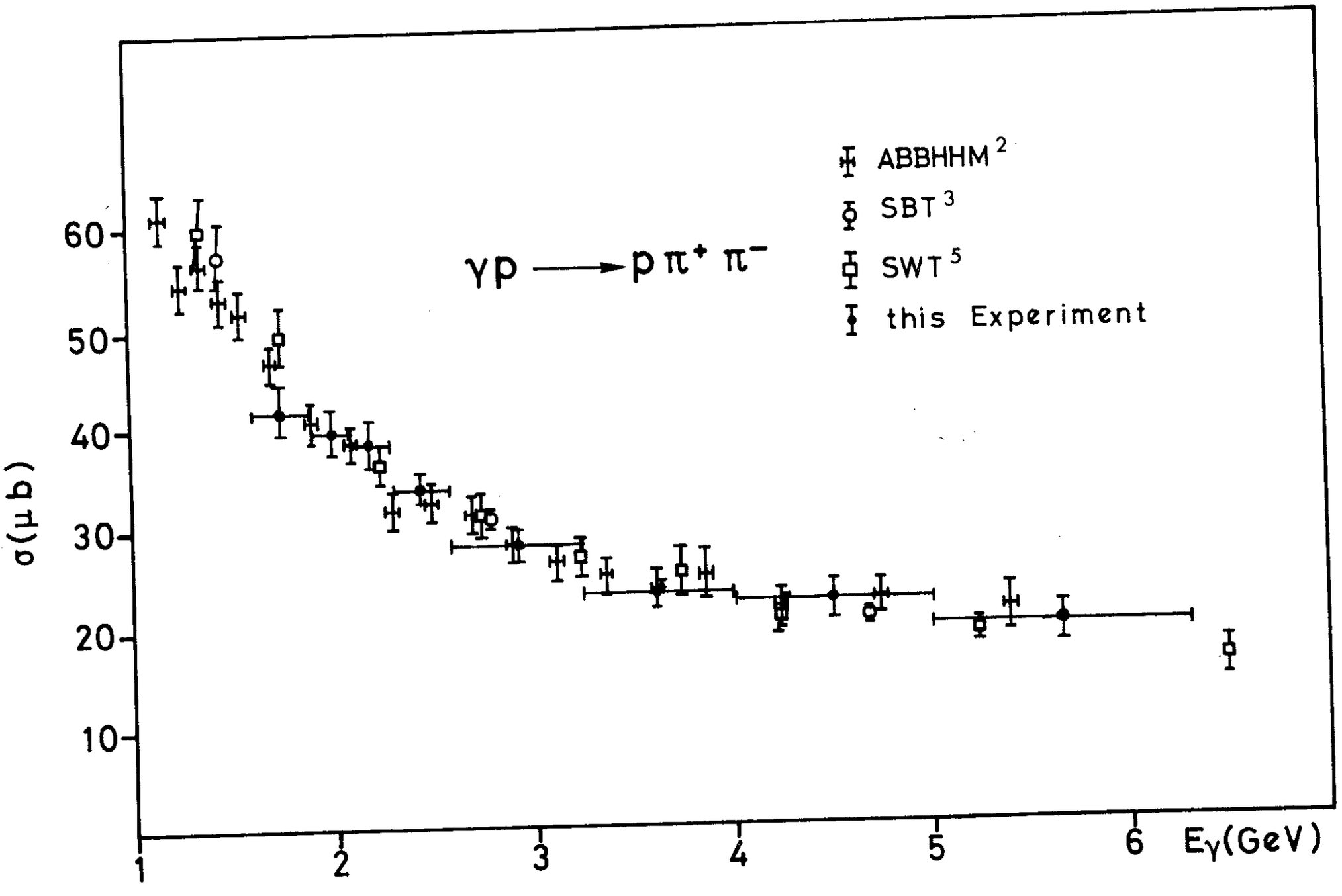
γp ⟶ p π⁺ π⁻
ABBHHM [2]
SBT [3]
SWT [5]
this Experiment
σ(μb)
60
50
40
30
20
10
1
2
3
4
5
6
Eγ(GeV)

Fig. 4

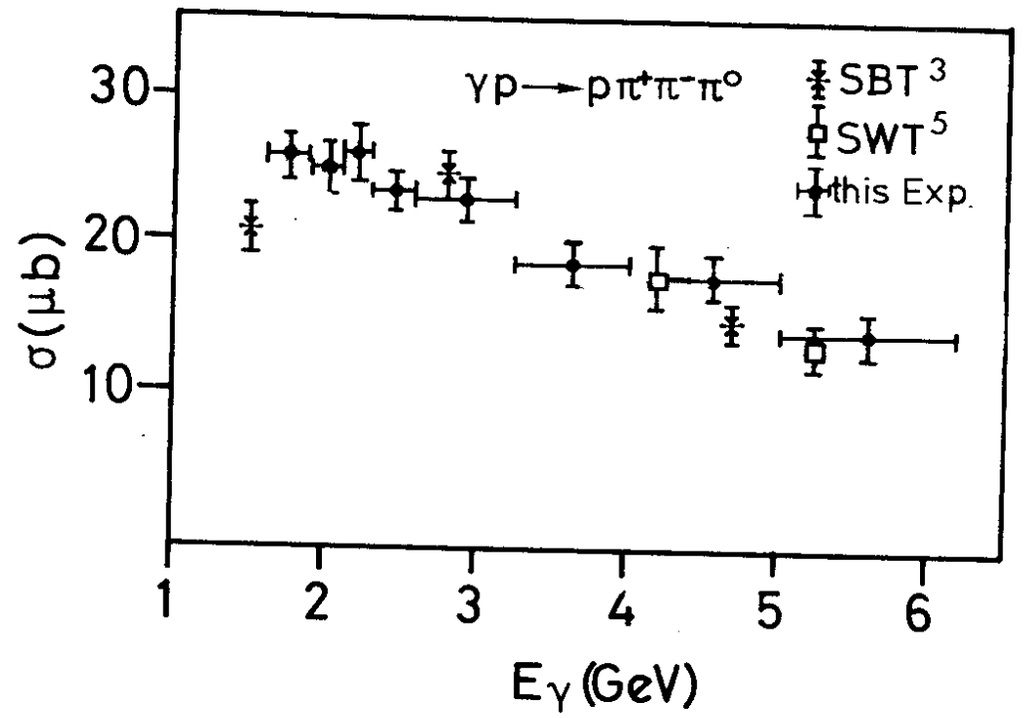
γp → pπ⁺π⁻π°
SBT [3]
SWT [5]
this Exp.
σ(μb)
30
20
10
1
2
3
4
5
6
Eγ (GeV)

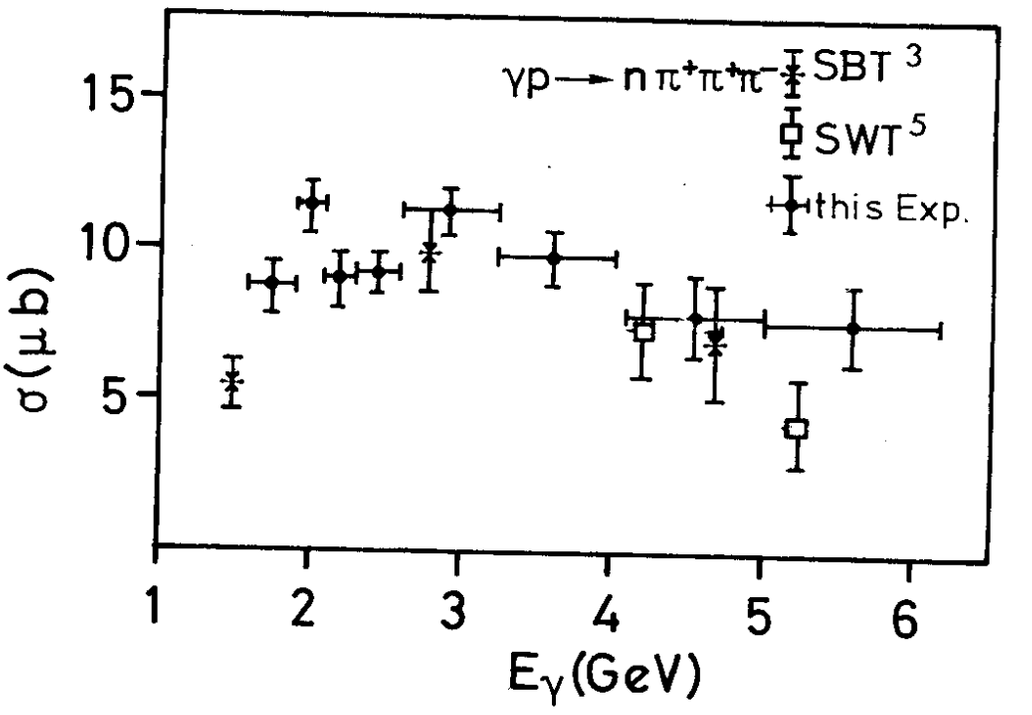
γp → nπ⁺π⁺π⁻
SBT [3]
SWT [5]
this Exp.
σ(μb)
15
10
5
1
2
3
4
5
6
Eγ (GeV)

Fig. 5

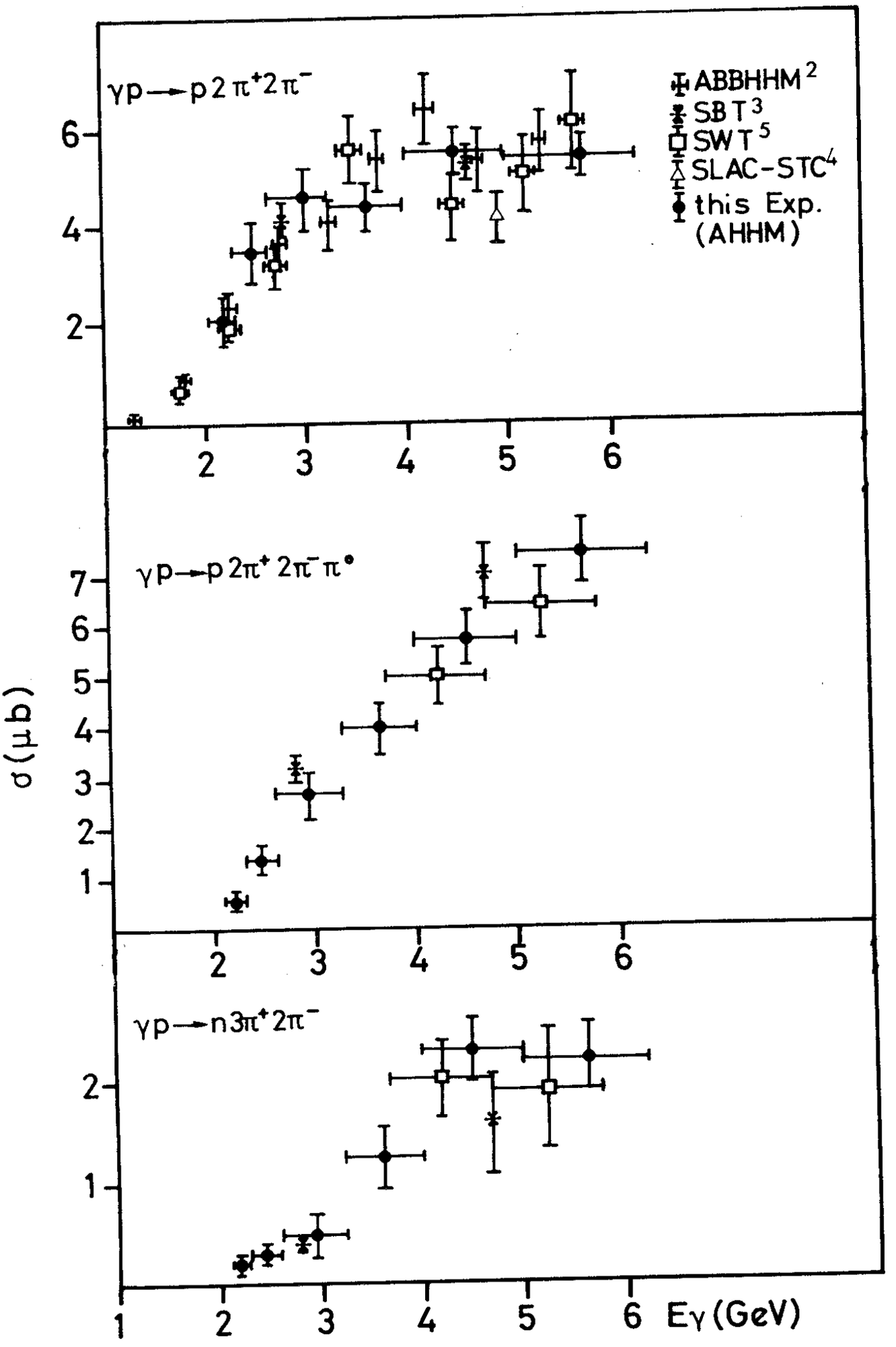
γp → p 2π⁺2π⁻
ABBHHM [2]
SBT [3]
SWT [5]
SLAC-STC [4]
this Exp. (AHHM)
γp → p 2π⁺ 2π⁻ π°
γp → n 3π⁺ 2π⁻
σ(μb)
Eγ (GeV)

Fig. 6

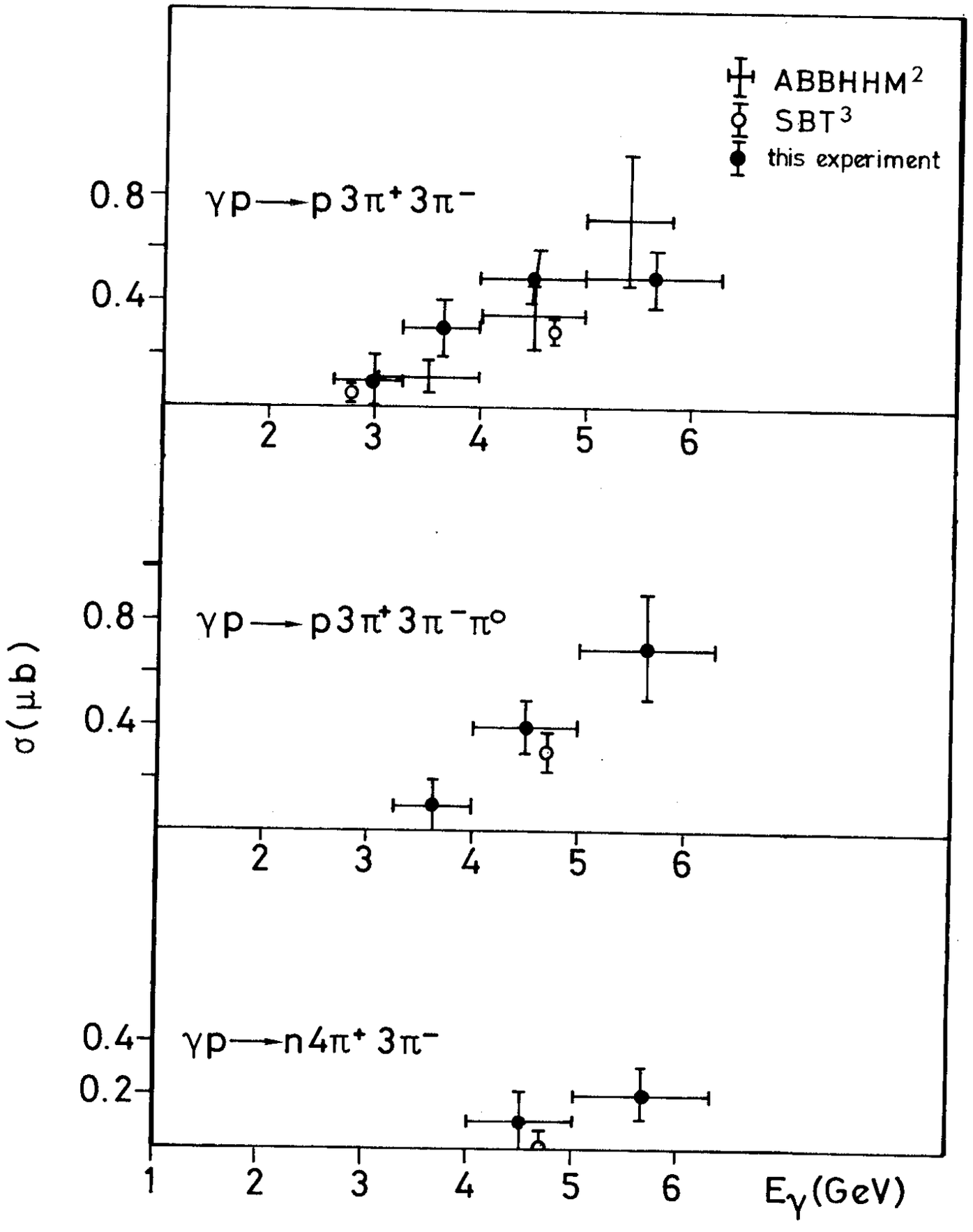
ABBHHM[2]
SBT[3]
this experiment
γp → p 3π⁺ 3π⁻
γp → p 3π⁺ 3π⁻π°
γp → n 4π⁺ 3π⁻
0.8
0.4
0.8
0.4
0.4
0.2
1
2
3
4
5
6
σ(μb)
Eγ(GeV)

Fig. 7

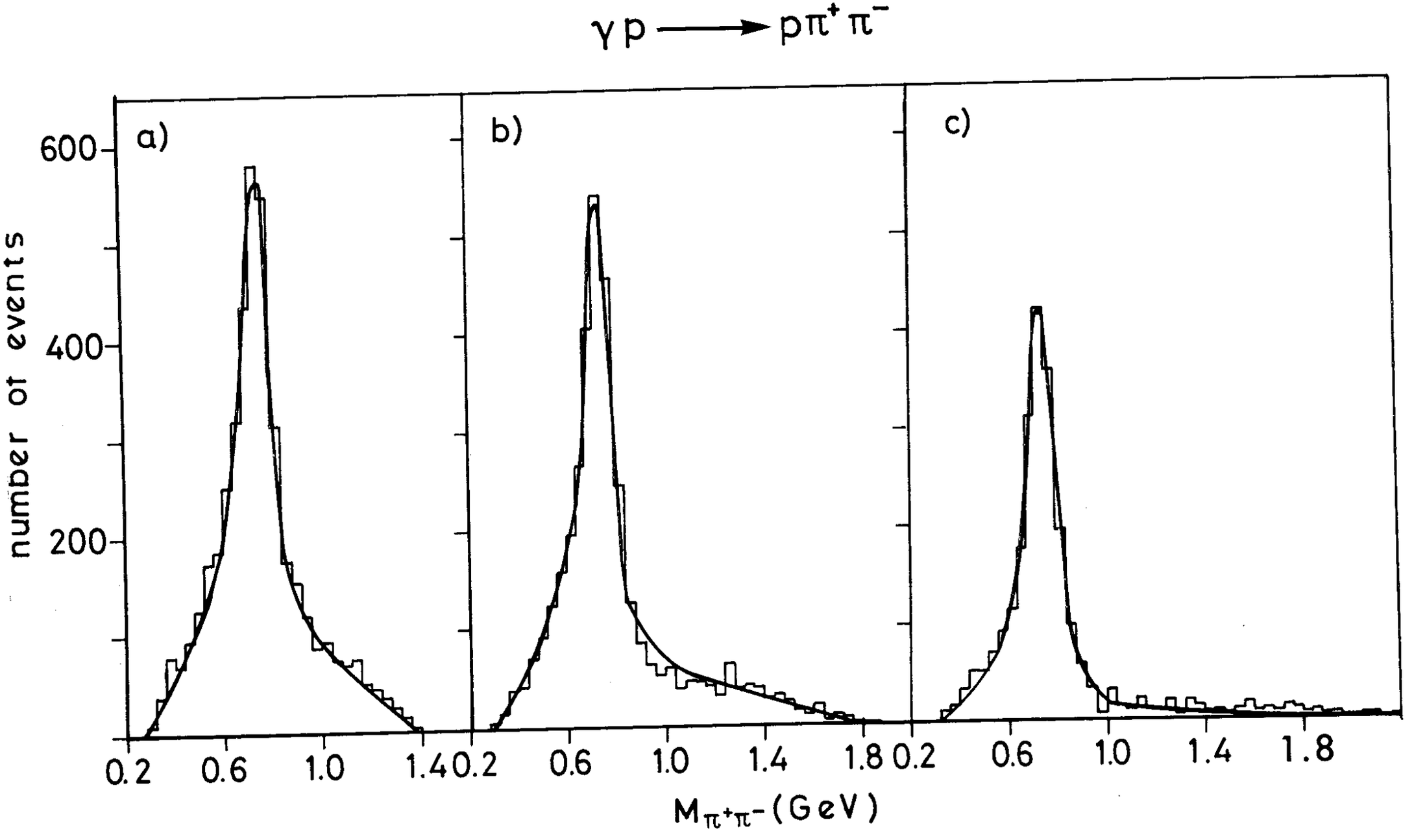

Fig. 8

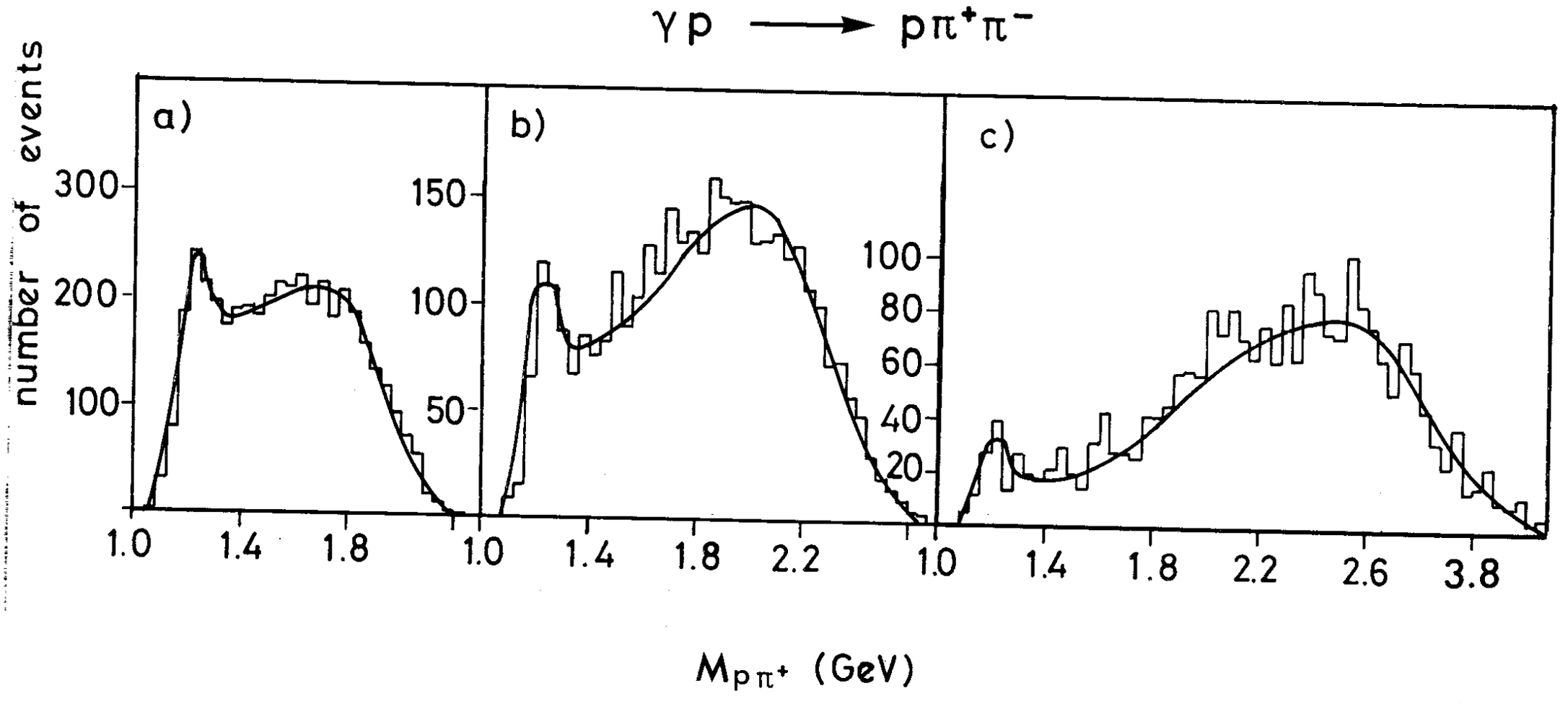
γp ⟶ pπ⁺π⁻
number of events
a)
b)
c)
300
200
100
150
100
50
100
80
60
40
20
1.0
1.4
1.8
1.0
1.4
1.8
2.2
1.0
1.4
1.8
2.2
2.6
3.8
Mpπ⁺ (GeV)

Fig. 9

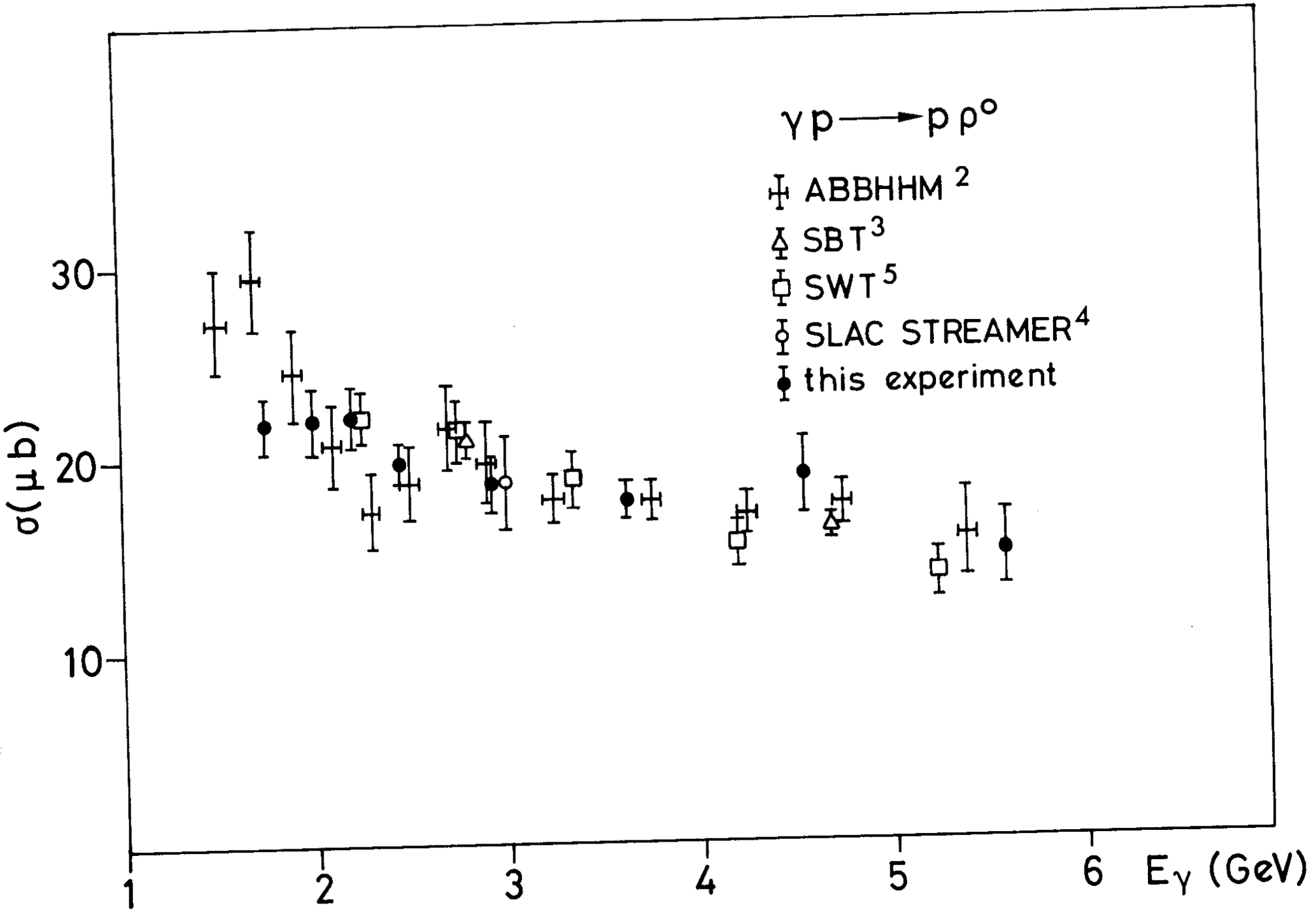
γp ⟶ pρ°
ABBHHM [2]
SBT [3]
SWT [5]
SLAC STREAMER [4]
this experiment
σ(μb)
30
20
10
1
2
3
4
5
6
Eγ (GeV)

Fig. 10

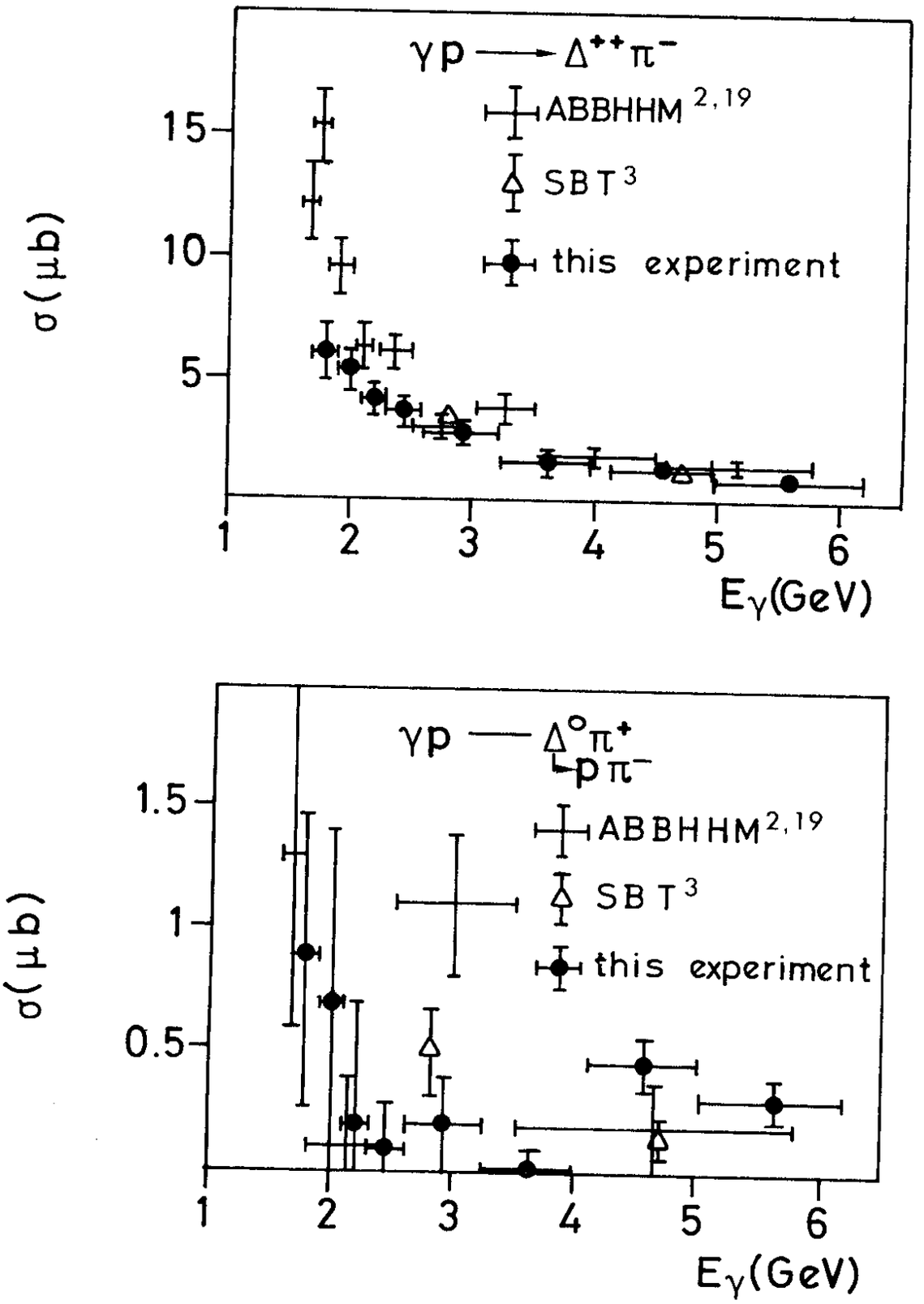
γp → Δ++π−
ABBHHM 2,19
SBT 3
this experiment
σ(μb)
15
10
5
1
2
3
4
5
6
Eγ(GeV)
γp — Δ°π+
↳pπ−
ABBHHM 2,19
SBT 3
this experiment
σ(μb)
1.5
1
0.5
1
2
3
4
5
6
Eγ(GeV)

Fig. 11

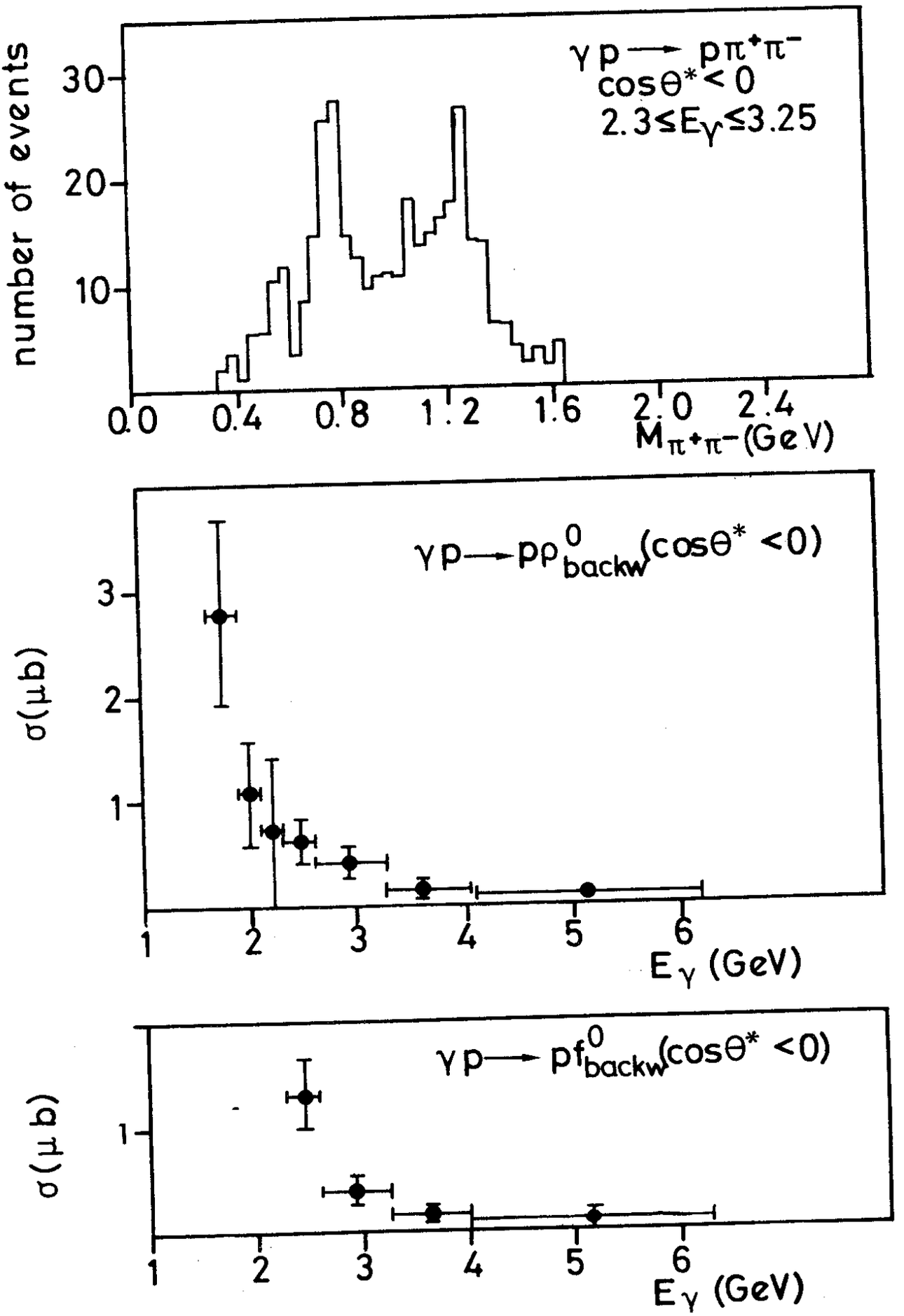
number of events
30
20
10
0.0
0.4
0.8
1.2
1.6
2.0
2.4
$M_{\pi^+\pi^-}$ (GeV)
$\gamma p \rightarrow p\pi^+\pi^-$
$\cos\theta^* < 0$
$2.3 \leq E_\gamma \leq 3.25$
$\sigma(\mu b)$
3
2
1
$\gamma p \rightarrow p\rho^0_{backw} (\cos\theta^* < 0)$
1
2
3
4
5
6
E_γ (GeV)
$\sigma(\mu b)$
1
$\gamma p \rightarrow p f^0_{backw} (\cos\theta^* < 0)$
1
2
3
4
5
6
E_γ (GeV)

Fig.12

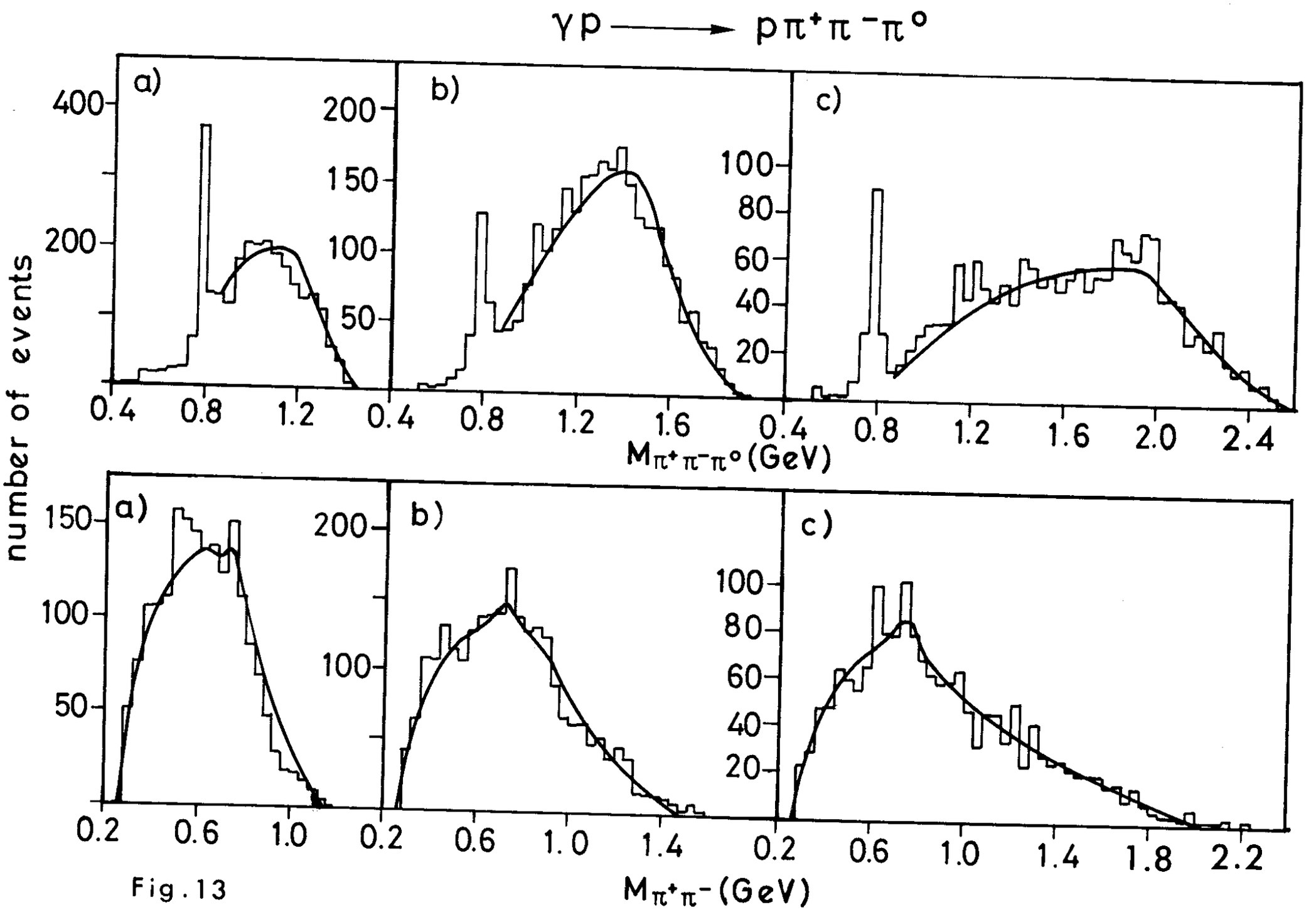
γp ⟶ pπ⁺π⁻π°
a)
b)
c)
number of events
400
200
150
100
50
80
60
40
20
0.4
0.8
1.2
1.6
2.0
2.4
Mπ⁺π⁻π° (GeV)
150
0.2
0.6
1.0
1.4
1.8
2.2
Mπ⁺π⁻ (GeV)

Fig. 13

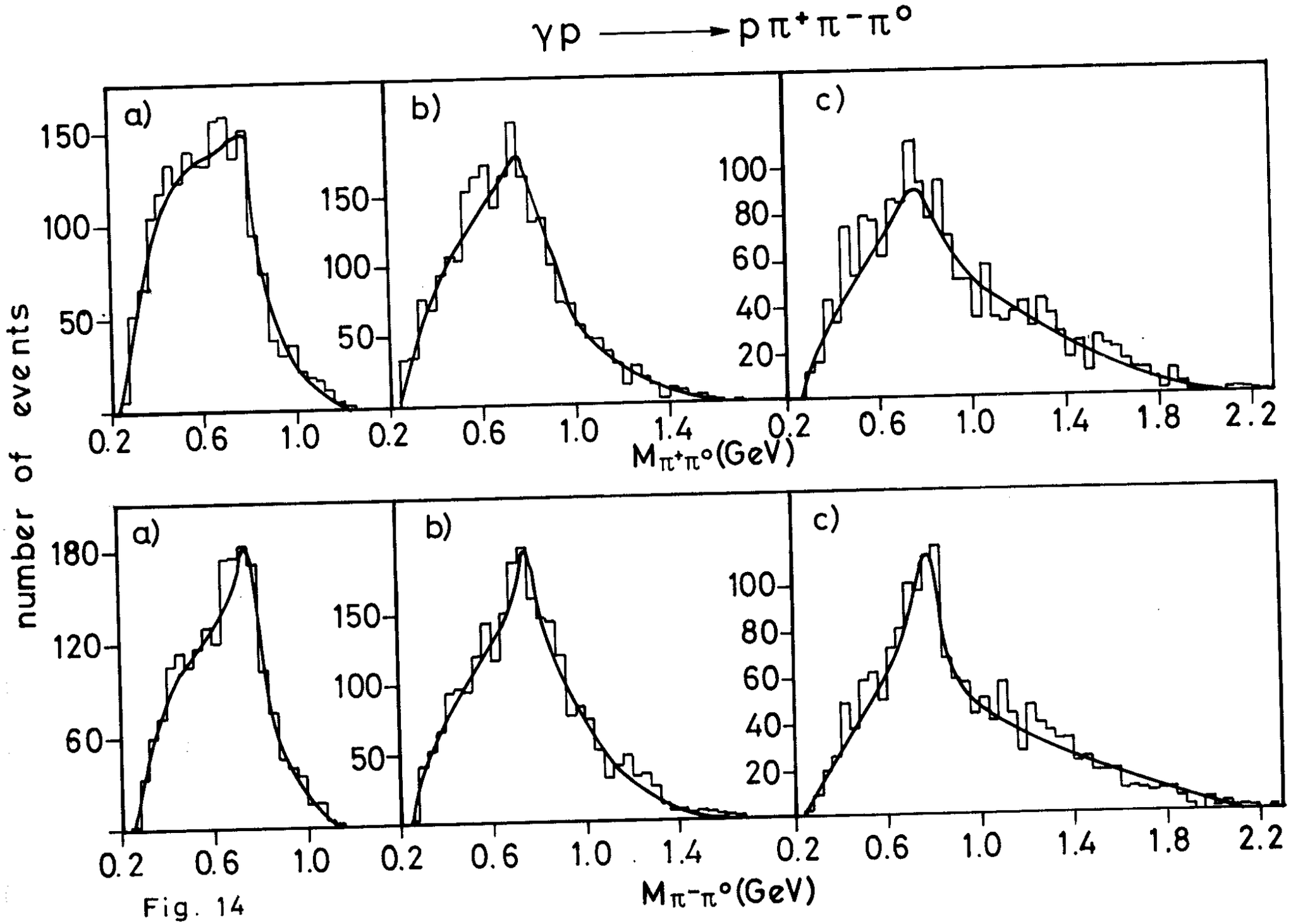

Fig. 14

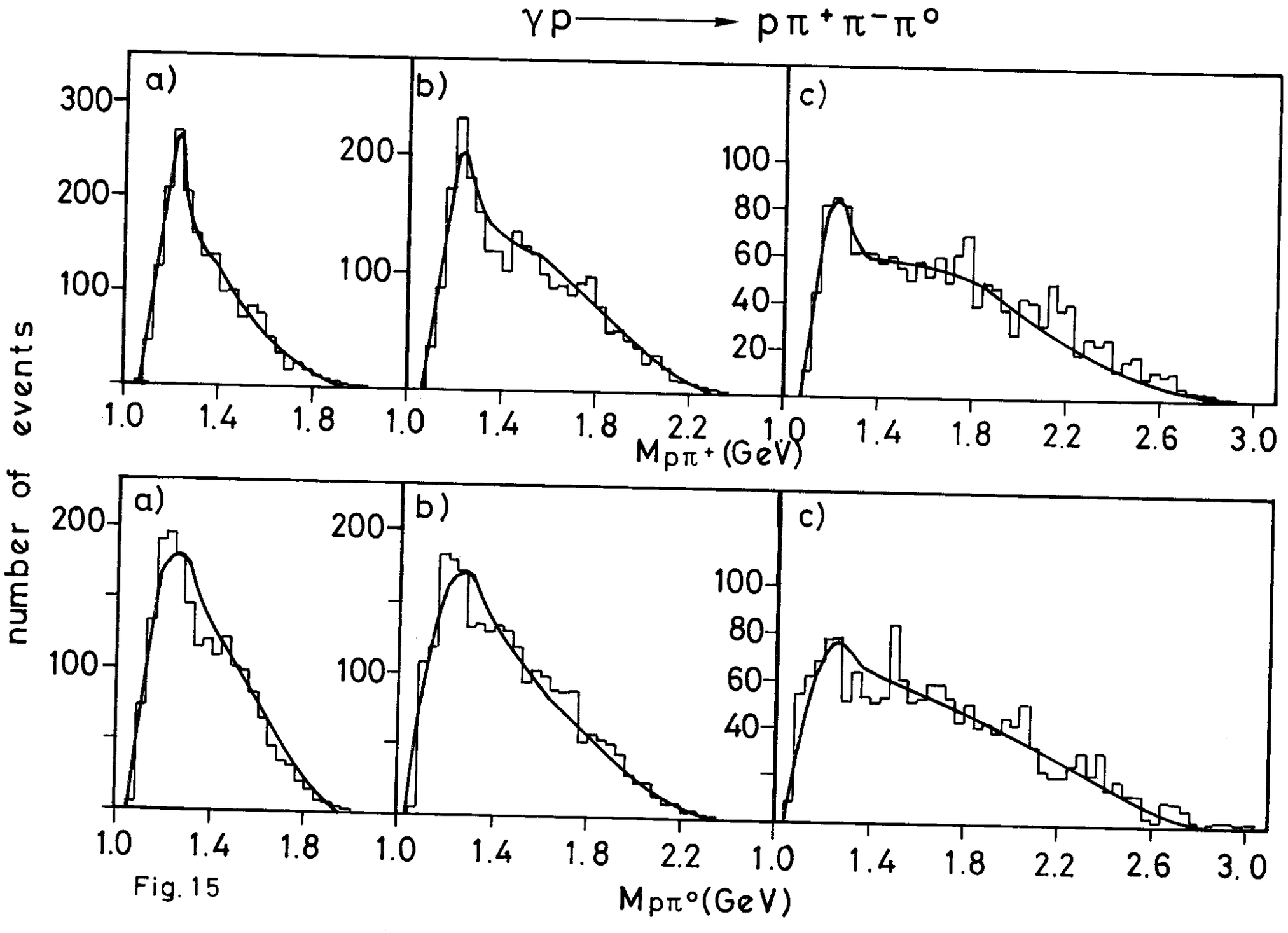
γp ⟶ pπ⁺π⁻π°
a)
b)
c)
300
200
100
200
100
100
80
60
40
20
1.0
1.4
1.8
1.0
1.4
1.8
2.2
1.0
1.4
1.8
2.2
2.6
3.0
Mpπ⁺(GeV)
number of events
a)
b)
c)
200
100
200
100
100
80
60
40
1.0
1.4
1.8
1.0
1.4
1.8
2.2
1.0
1.4
1.8
2.2
2.6
3.0
Mpπ°(GeV)

Fig. 15

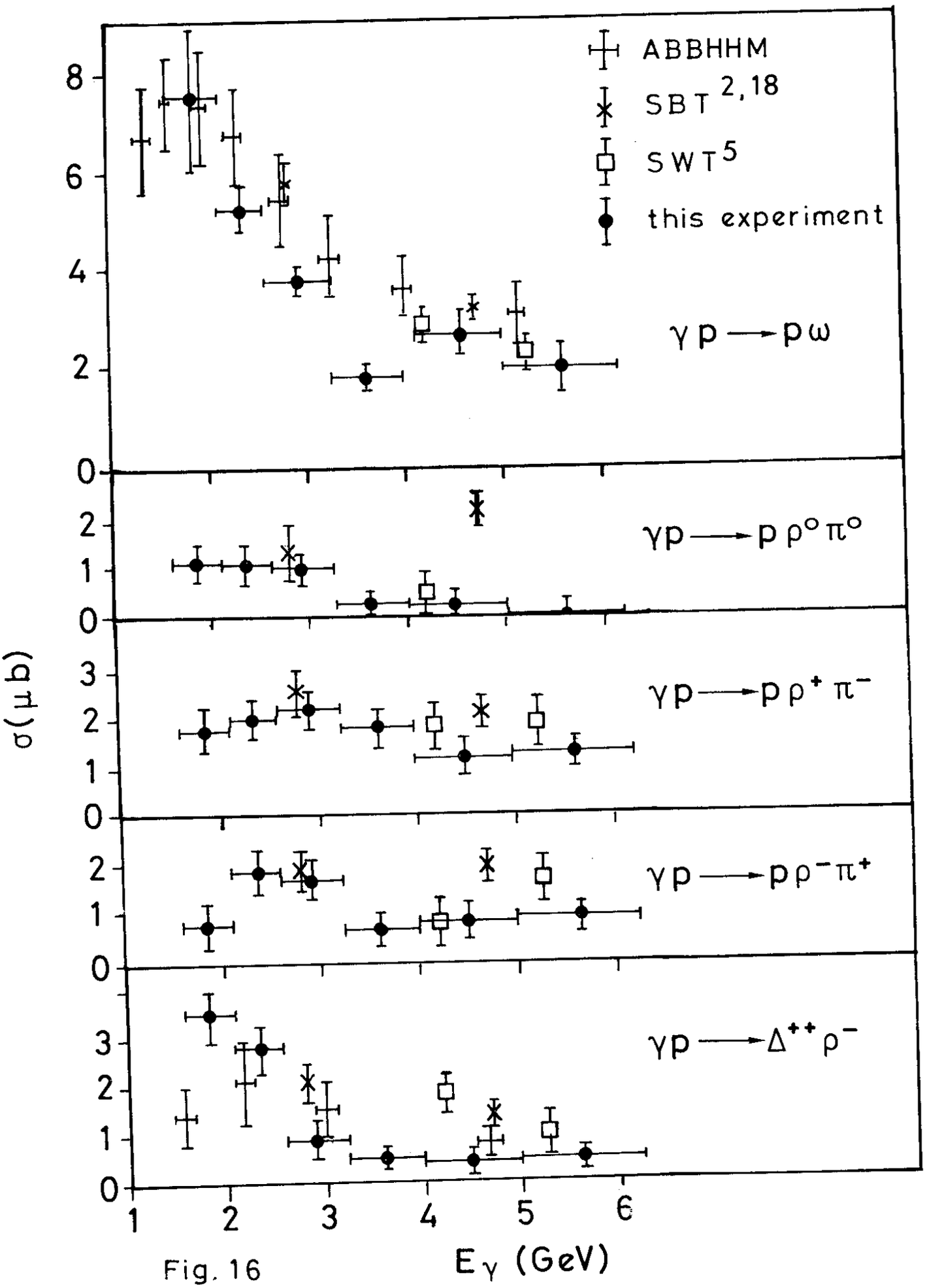
ABBHHM
SBT [2,18]
SWT [5]
this experiment
γp → pω
γp → pρ°π°
γp → pρ⁺π⁻
γp → pρ⁻π⁺
γp → Δ⁺⁺ρ⁻
σ(μb)
Eγ (GeV)

Fig. 16

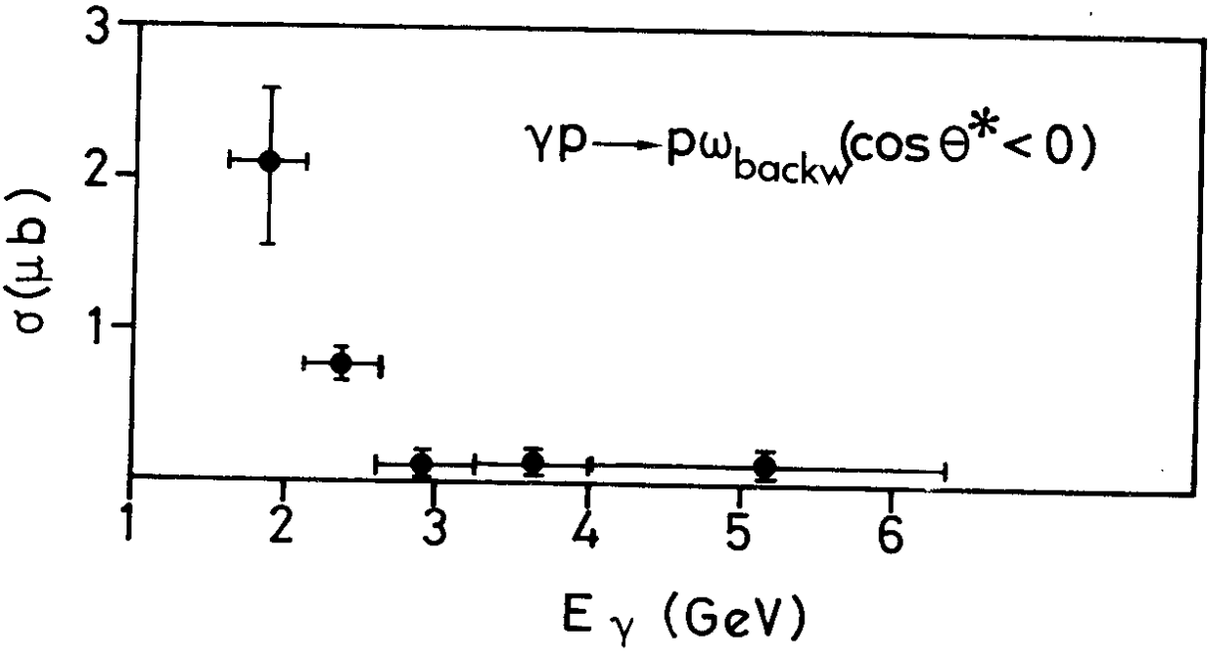

Fig. 17

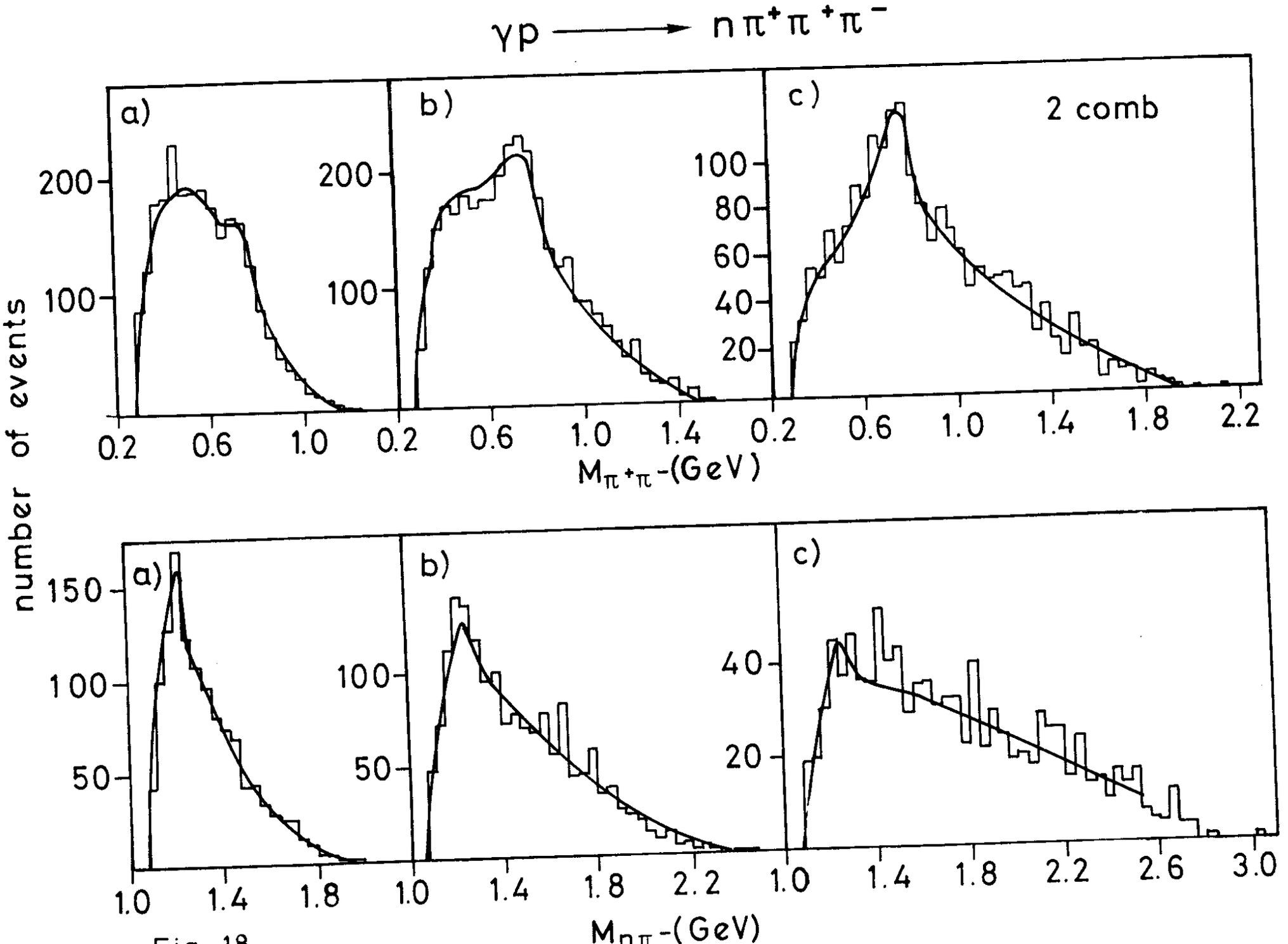

Fig. 18

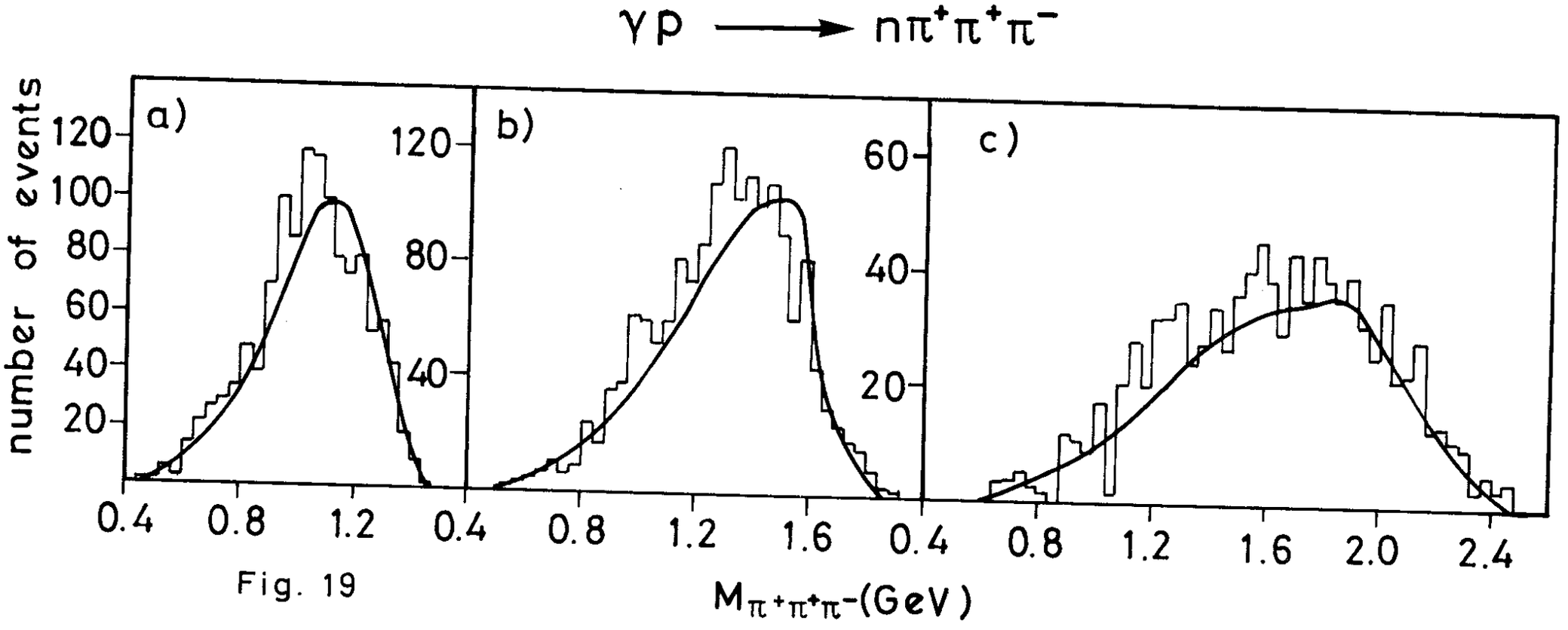
γp ⟶ nπ⁺π⁺π⁻
number of events
a)
b)
c)
120
100
80
60
40
20
120
80
40
60
40
20
0.4
0.8
1.2
0.4
0.8
1.2
1.6
0.4
0.8
1.2
1.6
2.0
2.4
Mπ⁺π⁺π⁻(GeV)

Fig. 19

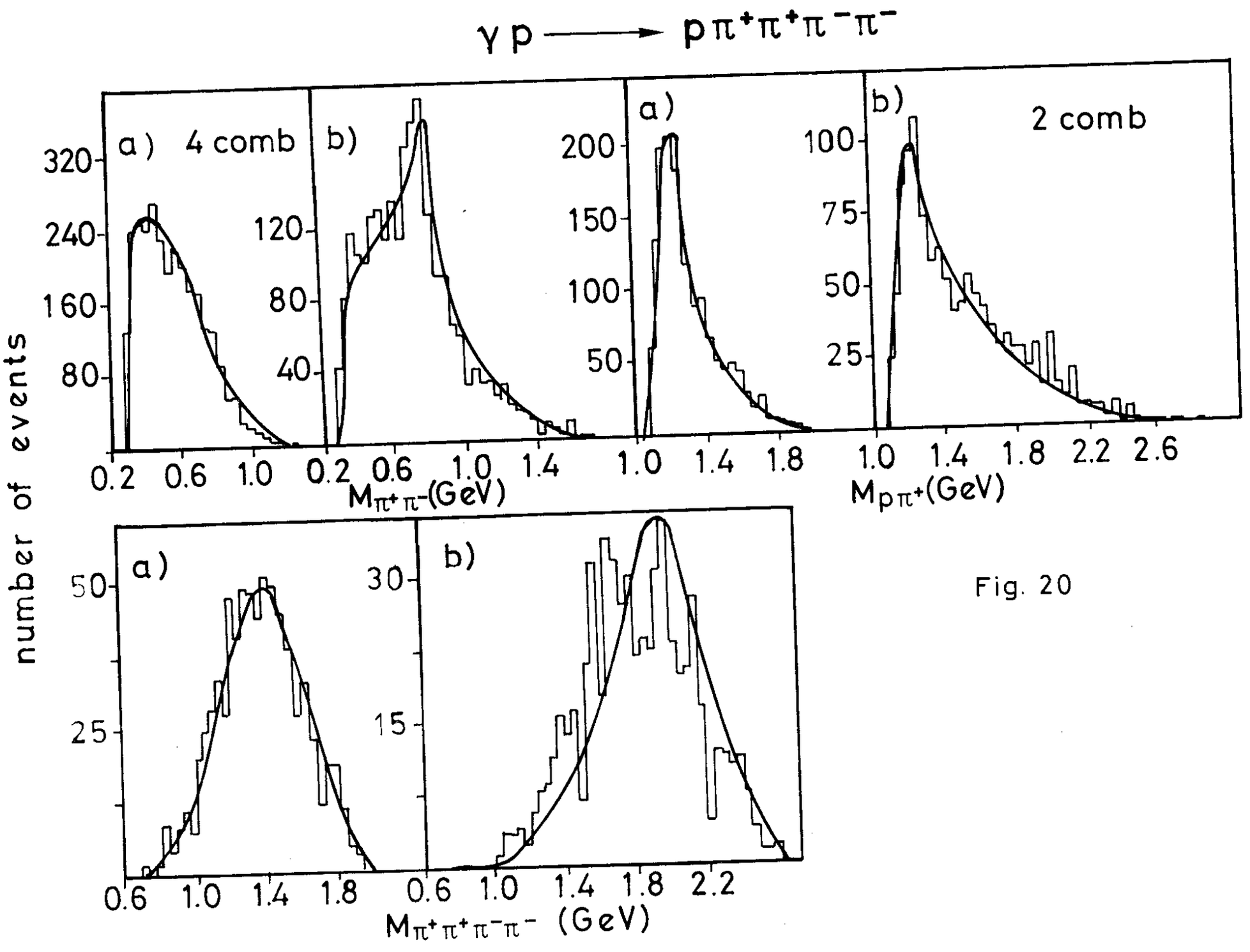
γ p ⟶ p π⁺π⁺π⁻π⁻
a) 4 comb
b)
a)
b) 2 comb
number of events
320
240
160
80
120
80
40
200
150
100
50
100
75
50
25
0.2 0.6 1.0
0.2 0.6 1.0 1.4
1.0 1.4 1.8
1.0 1.4 1.8 2.2 2.6
Mπ⁺π⁻(GeV)
Mpπ⁺(GeV)
a)
b)
50
25
30
15
0.6 1.0 1.4 1.8
0.6 1.0 1.4 1.8 2.2
Mπ⁺π⁺π⁻π⁻ (GeV)

Fig. 20

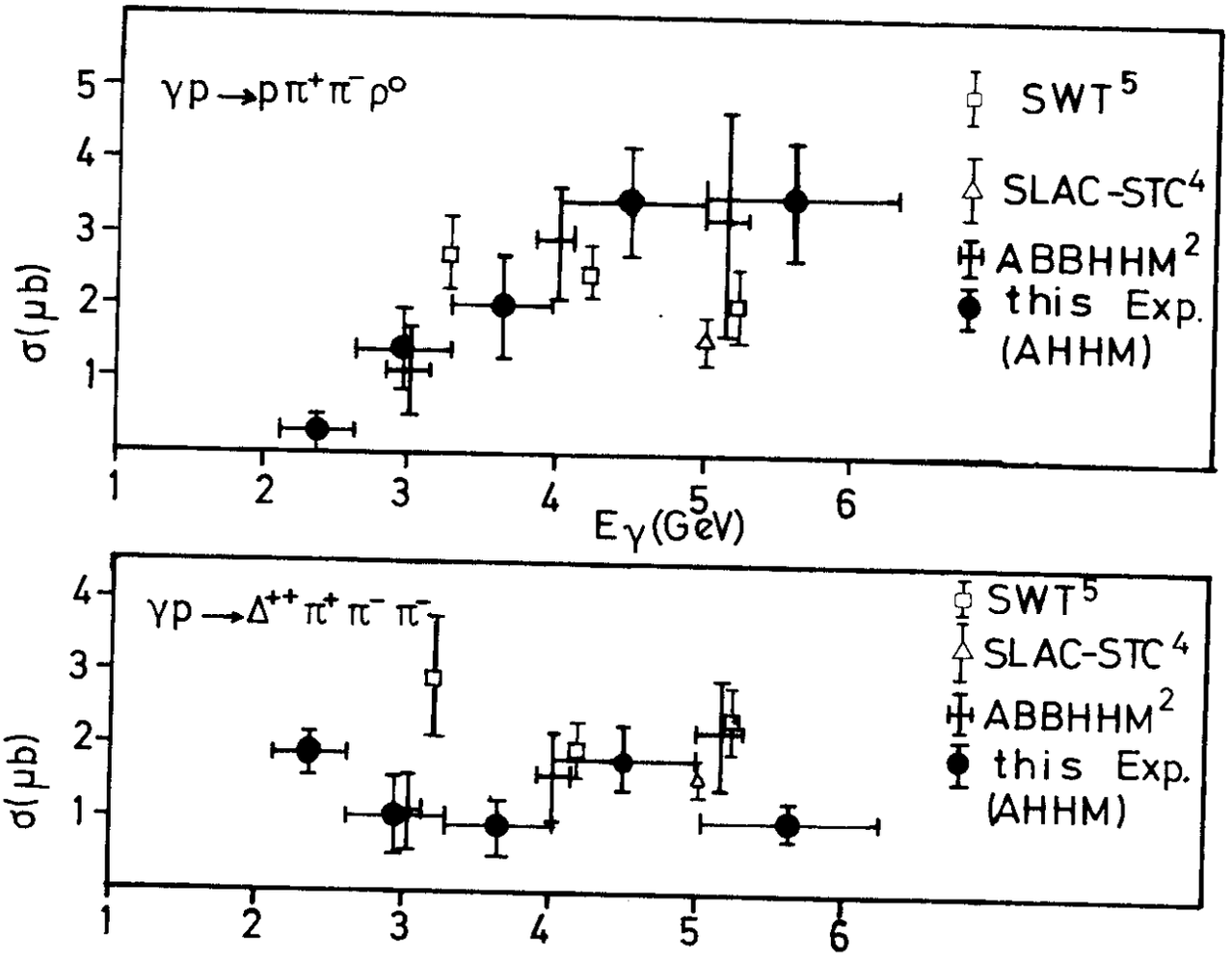
γp → pπ⁺π⁻ρ°
SWT⁵
SLAC-STC⁴
ABBHHM²
this Exp. (AHHM)
σ(μb)
Eγ(GeV)
γp → Δ⁺⁺π⁺π⁻π⁻
SWT⁵
SLAC-STC⁴
ABBHHM²
this Exp. (AHHM)
σ(μb)
Eγ (GeV)

Fig. 21

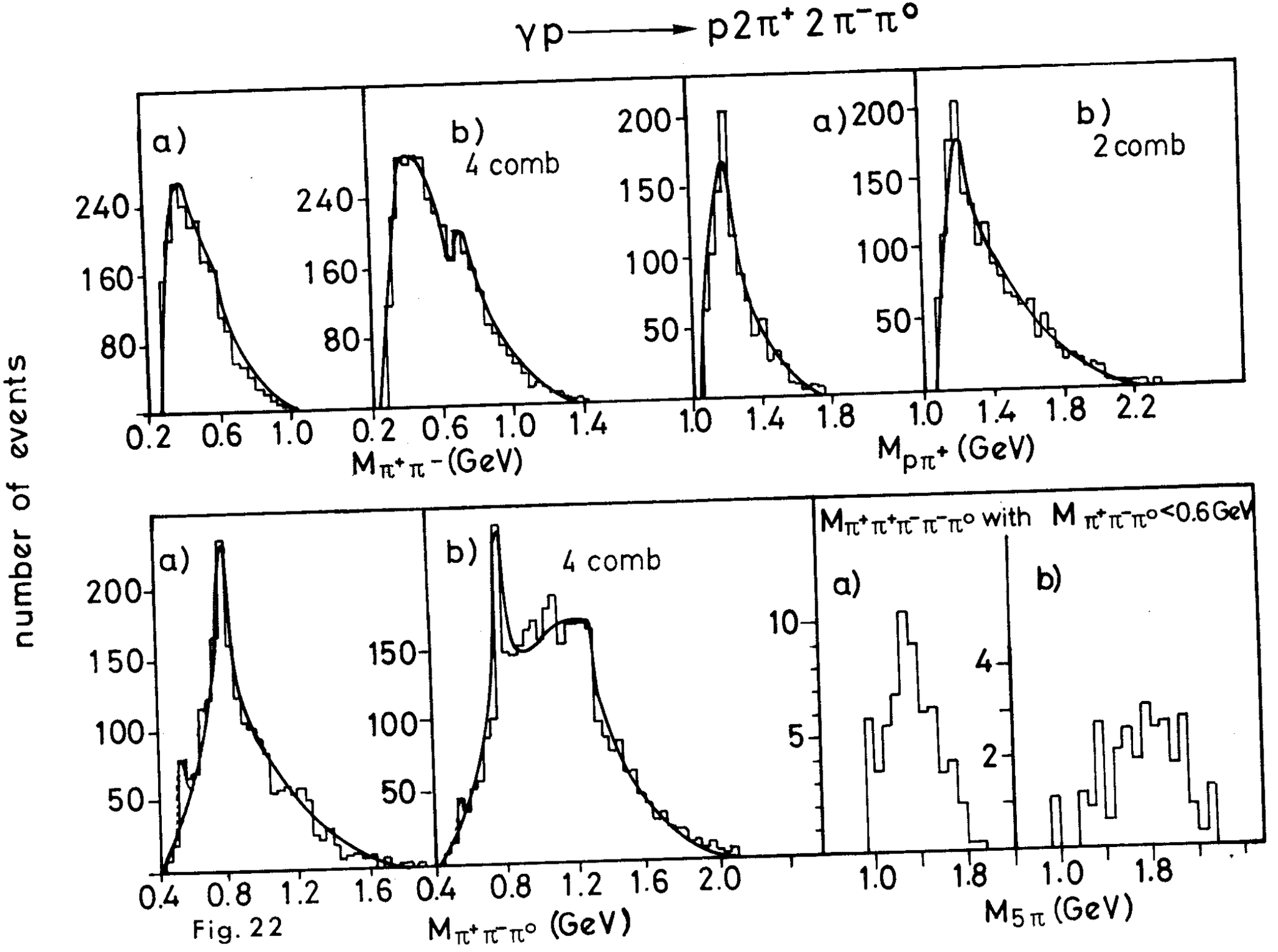
γp ⟶ p2π⁺2π⁻π°
number of events
a)
b)
4 comb
2 comb
$M_{\pi^+\pi^-}$ (GeV)
$M_{p\pi^+}$ (GeV)
$M_{\pi^+\pi^-\pi^\circ}$ (GeV)
$M_{5\pi}$ (GeV)
$M_{\pi^+\pi^+\pi^-\pi^-\pi^\circ}$ with $M_{\pi^+\pi^-\pi^\circ}$<0.6GeV

Fig. 22

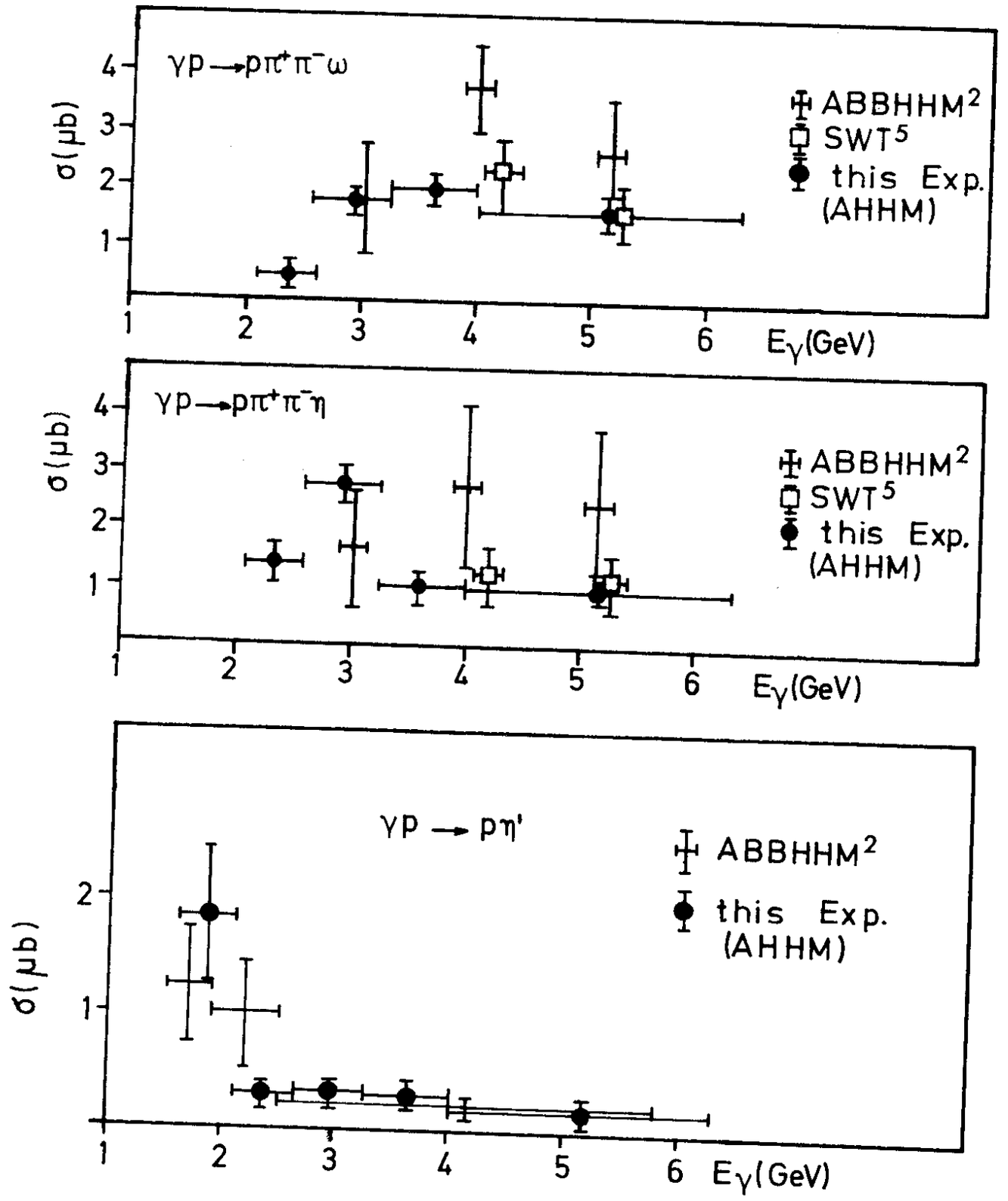
γp → pπ⁺π⁻ω
σ(μb)
ABBHHM²
SWT⁵
this Exp. (AHHM)
Eγ(GeV)
γp → pπ⁺π⁻η
σ(μb)
ABBHHM²
SWT⁵
this Exp. (AHHM)
Eγ(GeV)
γp → pη'
σ(μb)
ABBHHM²
this Exp. (AHHM)
Eγ(GeV)

Fig. 23

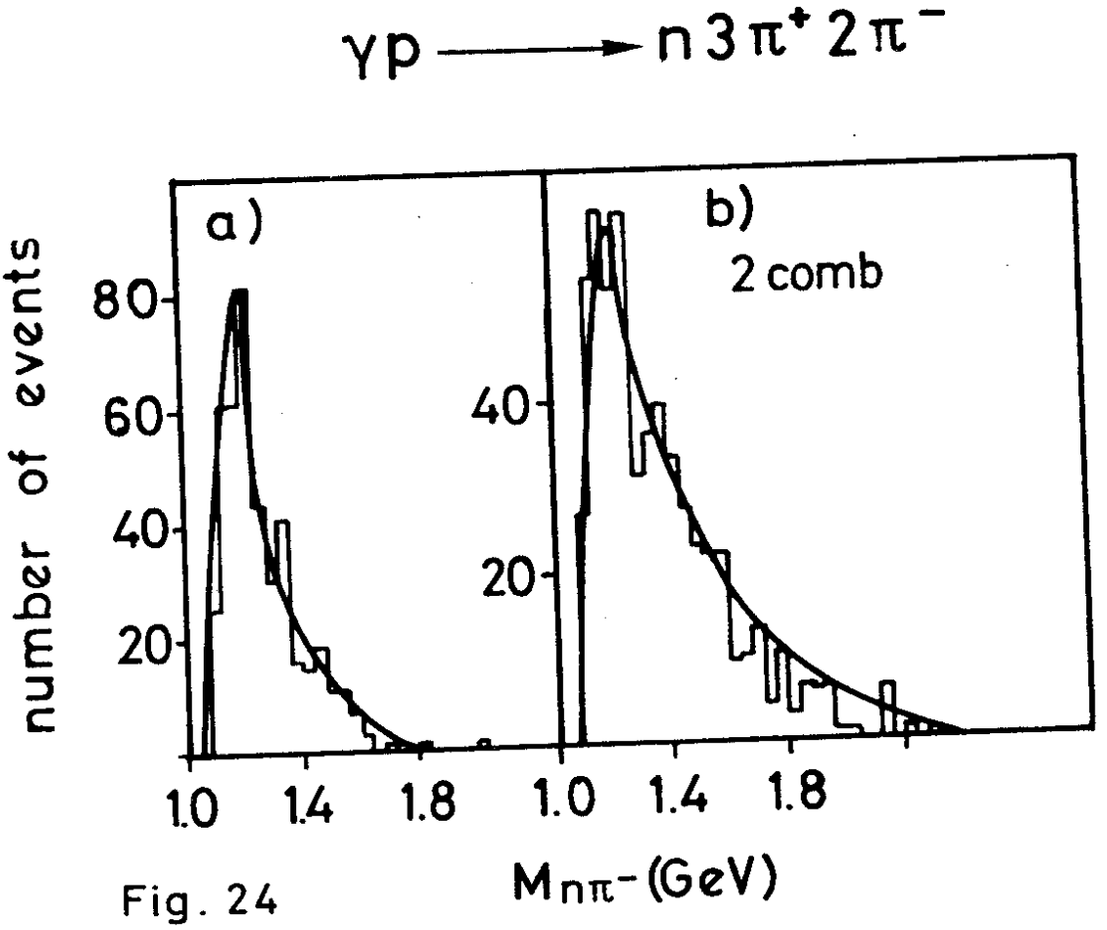
γp ⟶ n 3π⁺ 2π⁻
a)
b)
2 comb
number of events
80
60
40
20
40
20
1.0
1.4
1.8
1.0
1.4
1.8
Mnπ⁻ (GeV)

Fig. 24

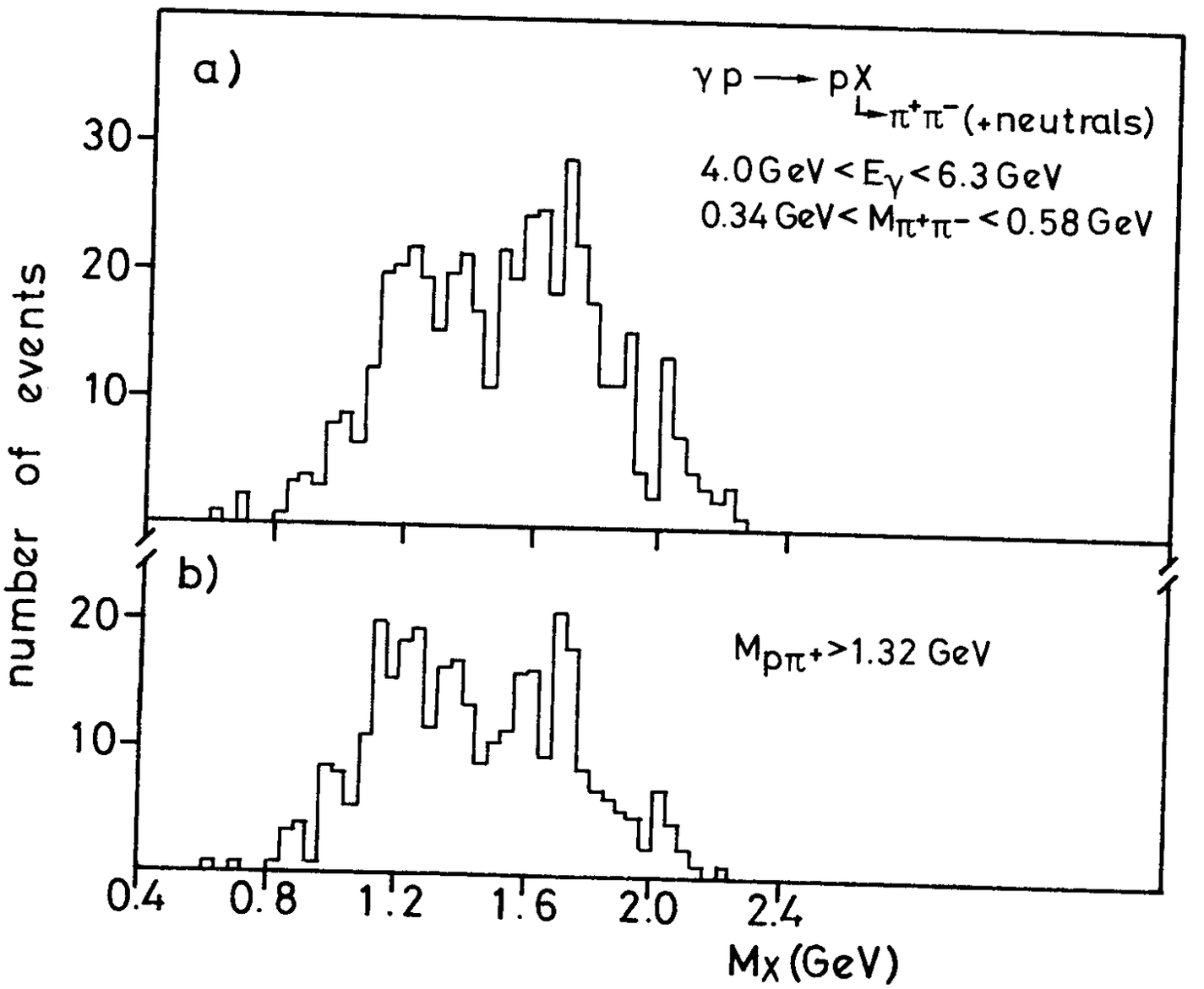
a)
γ p ⟶ pX
↳π⁺π⁻ (+neutrals)
4.0 GeV < Eγ < 6.3 GeV
0.34 GeV < Mπ⁺π⁻ < 0.58 GeV
30
20
10
b)
20
10
Mpπ⁺ > 1.32 GeV
number of events
0.4
0.8
1.2
1.6
2.0
2.4
MX (GeV)

Fig. 25